SASYR Symposium of Applied Science for Young Researchers

3rd Symposium of Applied Science for Young Researchers

SHORT PAPERS 2023

July 11 , 2023

3rd Symposium of Applied Science for Young Researchers

Short Papers

SASYR 2023

11 July 2023

Editors

Florbela P. Fernandes
Research Centre in Digitalization and Intelligent Robotics (CeDRI)
Instituto Politécnico de Bragança

Pedro Morais
Applied Artificial Intelligence Laboratory (2Ai)
Instituto Politécnico do Cávado e do Ave

Pedro Pinto
Applied Digital Transformation Laboratory (ADiT-LAB)
Instituto Politécnico de Viana do Castelo

Instituto Politécnico de Bragança — 2023
Campus de Santa Apolónia
5300-253 Bragança - Portugal
ISBN: 978-972-745-325-2

Book cover: Natália Santos, Instituto Politécnico do Cávado e do Ave

Welcome

These are the short papers proceedings of the 3rd Symposium of Applied Science for Young Researchers – SASYR. This scientific event welcomed works by junior researchers on any research topic covered by the following three research centers: ADiT-lab (from IPVC, Instituto Politécnico de Viana do Castelo), 2Ai (from IPCA, Instituto Politécnico do Cávado e do Ave) and CeDRI (from IPB, Instituto Politécnico de Bragança). The main objective of SASYR is to provide a friendly and relaxed environment for young researchers to present their work, discuss recent results, and develop new ideas. In this way, this event offered an opportunity for the ADiT-lab, 2Ai, and CeDRI research communities to gather synergies and promote collaborations, thus improving the quality of their research. The SASYR 2023 took place at Instituto Politécnico do Cávado e do Ave, Barcelos, Portugal, on the 11th of July, 2023.

The SASYR 2023 Organizing Committee,
Florbela P. Fernandes
Pedro Morais
Pedro Pinto

Committees

Organizing Committee

Florbela Fernandes, CeDRI, Instituto Politécnico de Bragança
Pedro Morais, 2Ai, Instituto Politécnico do Cávado e do Ave
Pedro Pinto, ADiT-lab, Instituto Politécnico de Viana do Castelo

Advisory Committee

Ana Pereira, CeDRI, Instituto Politécnico de Bragança
José Lima, CeDRI, Instituto Politécnico de Bragança
Paulo Leitão, CeDRI, Instituto Politécnico de Bragança
João L. Vilaça, 2Ai, Instituto Politécnico do Cávado e Ave
António Miguel Cruz, ADiT-lab, Instituto Politécnico de Viana do Castelo
Jorge Garcia, ADiT-lab, Instituto Politécnico de Viana do Castelo

Technical Support

Carla Fontes, Instituto Politécnico de Bragança
Clarisse Pais, Instituto Politécnico de Bragança
Pedro Oliveira, Instituto Politécnico de Bragança
Susana Carvalho, Instituto Politécnico do Cávado e do Ave
Silvestre Malta, Instituto Politécnico de Viana do Castelo

Scientific Committee

Alberto Simões, 2Ai, Instituto Politécnico do Cávado e do Ave
Ana Isabel Pereira, CeDRI, Instituto Poliécnico de Bragança
André Mendes, CeDRI, Instituto Poliécnico de Bragança
Andreia Teixeira, ADiT-lab, Instituto Politécnico de Viana do Castelo
Ângela Ferreira, CeDRI, Instituto Poliécnico de Bragança
Ângela Silva, ADiT-lab, Instituto Politécnico de Viana do Castelo
António Cruz, ADiT-lab, Instituto Politécnico de Viana do Castelo
Antonio Moreira, 2Ai, Instituto Politécnico do Cávado e do Ave
Carla Soares Geraldes, CeDRI, Instituto Poliécnico de Bragança
Carlos Abreu, ADiT-lab, Instituto Politécnico de Viana do Castelo
Cátia Alves, 2Ai, Instituto Politécnico do Cávado e do Ave
Clara Vaz, CeDRI, Instituto Poliécnico de Bragança
Daniel Miranda, 2Ai, Instituto Politécnico do Cávado e do Ave
Diogo Lopes, 2Ai, Instituto Politécnico do Cávado e do Ave
Duarte Duque, 2Ai, Instituto Politécnico do Cávado e do Ave
Estela Vilhena, 2Ai, Instituto Politécnico do Cávado e do Ave

Eva Oliveira, 2Ai, Instituto Politécnico do Cávado e do Ave
Fernando Monteiro, CeDRI, Instituto Poliécnico de Bragança
Florbela P. Fernandes, CeDRI, Instituto Poliécnico de Bragança
João Carlos Silva, 2Ai, Instituto Politécnico do Cávado e do Ave
João L. Vilaça, 2Ai, Instituto Politécnico do Cávado e do Ave
João Paulo Coelho, Instituto Poliécnico de Bragança
João Paulo Teixeira, CeDRI, Instituto Poliécnico de Bragança
Joaquim Gonçalves, 2Ai, Instituto Politécnico do Cávado e do Ave
Jorge Ribeiro, ADiT-lab, Instituto Politécnico de Viana do Castelo
Jose Henrique Brito, 2Ai, Instituto Politécnico do Cávado e do Ave
José Lima, CeDRI, Instituto Poliécnico de Bragança
Jose Rufino, CeDRI, Instituto Poliécnico de Bragança
Luis Ferreira, 2Ai, Instituto Politécnico do Cávado e do Ave
Luís Teófilo, ADiT-lab, Instituto Politécnico de Viana do Castelo
Luisa Jorge, CeDRI, Instituto Poliécnico de Bragança
Manuela Cruz-Cunha, 2Ai, Instituto Politécnico do Cávado e do Ave
Maria F. Pacheco, CeDRI, Instituto Poliécnico de Bragança
Maria Mourão, ADiT-lab, Instituto Politécnico de Viana do Castelo
Natália Rego, 2Ai, Instituto Politécnico do Cávado e do Ave
Nuno Lopes, 2Ai, Instituto Politécnico do Cávado e do Ave
Óscar Ribeiro, 2Ai, Instituto Politécnico do Cávado e do Ave
Patrícia Leite, 2Ai, Instituto Politécnico do Cávado e do Ave
Paula Alexandra Rego, ADiT-lab, Instituto Politécnico de Viana do Castelo
Paulo Costa, ADiT-lab, Instituto Politécnico de Viana do Castelo
Paulo Leitao, CeDRI, Instituto Poliécnico de Bragança
Paulo Matos, CeDRI, Instituto Poliécnico de Bragança
Pedro Morais, 2Ai, Instituto Politécnico do Cávado e do Ave
Pedro Pinto, ADiT-lab, Instituto Politécnico de Viana do Castelo
Pedro Rodrigues, CeDRI, Instituto Poliécnico de Bragança
Rui Pedro Lopes, CeDRI, Instituto Poliécnico de Bragança
Sara Paiva, ADiT-lab, Instituto Politécnico de Viana do Castelo
Sérgio Lopes, ADiT-lab, Instituto Politécnico de Viana do Castelo
Teresa Abreu, 2Ai, Instituto Politécnico do Cávado e do Ave
Tiago Pedrosa, CeDRI, Instituto Poliécnico de Bragança
Vítor Carvalho, 2Ai, Instituto Politécnico do Cávado e do Ave

Table of Contents

Thermoplastic Polyurethane gradient deformation monitoring system used in helmets for Deformational Plagiocephaly

Sérgio G. Pereira[1], Fernando Veloso[1], Tiago H. Barros[1], Pedro Lobo[1], Pedro Morais[1], and João L. Vilaça[1]

Instituto Politécnico do Cávado e do Ave, IPCA, Portugal
sfpereira@ipca.pt, fveloso@ipca.pt, tbarros@ipca.pt, pjlobo@ipca.pt, pmorais@ipca.pt, jvilaca@ipca.pt

Abstract. Deformational Plagiocephaly (PD) is a common medical condition in children up to the age of 2. The deformity can be corrected using good practices recommended by the medical staff, however, in more severe cases, physical therapy is required. In this sense, cranial orthoses are mostly used to correct the deformity. However, the standard solutions do not quantify the treatment and are mostly produced through manually-based fabrication processes. Compression experiments were performed with the thermoplastic polyurethane (TPU) material and it was found that the greater the internal thickness of the material, the more force is required to make a displacement. Furthermore, we were able to obtain a linear model for the foams that characterizes the magnetic field obtained by the magnet as a function of displacement for 3 different types of internal thickness. Overall, the solution presented by us presents a huge potential to create a cranial deformation monitoring process.

Keywords: Deformational plagiocephaly · Magnetic sensor · Thermoplastic polyurethane compression.

1 Introduction

The Deformational Plagiocephaly (DP) continues to receive special attention in the medical area. This condition is characterized by an assymetry of the head shape [1] and, in most of the cases, physiotherapy treatment is realized. In severe cases, cranial orthoses are used to correct throughout the time the head growing, correcting its shape [2].

Most orthoses are constructed by a semi-rigid styrene-outer shell thermobonded to an inner lining of a polyurethane and are adapted to the patient's head [3]. In this sense, studies have been developed on helmets with dynamic materials (e.g. TPU) that adapt to the constant growth/displacement of the head depending on the force exerted [4]. However, the lattice structure developed in this study does not have a system for the monitoring of the compression applied on the infant´s head.

For this, the objective of this work is the development of a methodology capable of monitoring the local compression applied by the structure in the infant´s head by correlating the compression displacement of that lattice structure and the corresponding exerted force.

2 Experiments and Results

The first experiments involve three different homogeneous lattices. The main difference with this lattice is the internal density, which is given by the thickness of the pillars, as we can see in Fig. 1.

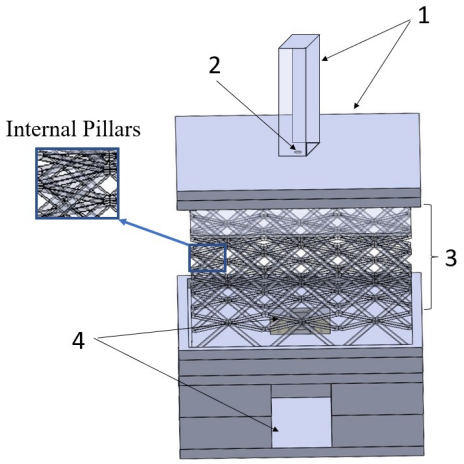

Fig. 1: Setup of experiment.

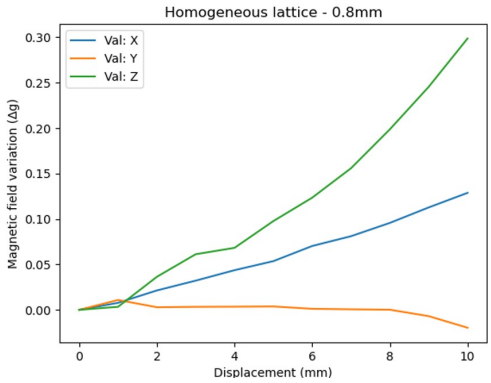

Fig. 2: Sensory response to magnetic field variation in 0.8mm homogeneous lattice.

The goal of this experiment is to correlate the magnetic field with the deformation of the gradient depending on its internal composition and for this, we create the setup present in Fig. 1. In 1, we see a tool drawn in SolidWorks (Massachusetts, United States) which will be used to apply compression to the gradient (3). This tool has a cavity (2) where the magnet will be inserted to stay in contact with the gradient (3). In 4, we can see the idealized support for the LIS3MDL sensor, this support allows the gradient to rest centrally on the sensor and has a side opening for the exit of the cables connected to the sensor.

We will apply with the compression displacements from 1mm to 7mm and record the magnetic field values to create a calibration curve for each homogeneous foam. For this, first, we take 100 samples from the initial position (0mm) and average them, then we do a 1mm shift and average over 100 more samples collected, then we see the variation of the magnetic field (Δg), which will be the difference between the average of the 100 samples of the displacement of 1mm in relation to the initial state (0mm). This process, will be repeated up to 7mm.

Table 1: Force required to exert displacement on homogeneous lattices.

Table	**Force (N)**		
Displacement (mm)	***0.8mm***	***1.4mm***	***2.0mm***
0	0	0	0
1	0.163	1.540	2.495
2	0.309	3.042	8.886
3	0.421	4.364	15.707
4	0.546	5.467	21.332
5	0.640	6.292	25.995
6	0.834	7.073	29.892
7	0.888	7.737	33.380

The magnetic sensor has 3 cartesian axes and each one is sensitive to the magnetic field, and from Fig. 2, we can see that the coordinate that has more sensitivity in our project is the 'Z', which makes total sense because we moved the magnet vertically to the sensor.

Furthermore, Table 1 also allows us to conclude that the force required to create the same deformation in the lattice, will be greater depending on the internal thickness of the pillars.

References

1. J. J. Xia, K. A. Kennedy, J. F. Teichgraeber, K. Q. Wu, J. B. Baumgartner, and J. Gateno. Nonsurgical Treatment of Deformational Plagiocephaly A Systematic Review. *Behav Biomed Mater*, 2008.
2. A. D. Inchingolo. A Systematic Review of Positional Plagiocephaly Prevention Methods for Patients in Development. *Applied Sciences*, 12(21):11172, Nov. 2022.
3. M. Geoffroy, J. Gardanand J. Goodnough, and J. Mattie. CASE REPORT Cranial Remodeling Orthosis for Infantile Plagiocephaly Created Through a 3D Scan, Topological Optimization, and 3D Printing Process. 2018.
4. F. Veloso, D. Miranda, P. Morais, H. R. Torres, B. Oliveira, J. Correia-Pinto, A. C. M. Pinho, and J. L. Vilaça. Study of the compression behavior of functionally graded lattice for customized cranial remodeling orthosis. *Behav Biomed Mater*, 130, Jun. 2022.

Printable piezoresistive polymer composites for biomedical applications

E. Pimentel[1,2,3] P. Costa,[2] J. L. Vilaça,[1,3] C. M. Costa,[2,5,6] S. Lanceros-Méndez[2,4,5,7], and D. Miranda[1,3]

[1] 2Ai- School of Technology, IPCA, 4750-810 Barcelos, Portugal
[2] Physics Centre of Minho and Porto Universities (CF-UM-UP), University of Minho, 4710-057 Braga,Portugal
[3] LASI – Associate Laboratory of Intelligent Systems, Guimarães, Portugal
[4] BCMaterials, Basque Center for Materials, Applications and Nanostructures, UPV/EHU Science Park, 48940 Leioa, Spain
[5] Laboratory of Physics for Materials and Emergent Technologies, LapMET, University of Minho, 4710-057 Braga, Portugal
[6] IB-S Institute of Science and Innovation for Sustainability, Universidade do Minho 4710-057, Braga, Portugal
[7] IKERBASQUE, Basque Foundation for Science, 48009 Bilbao, Spain
epimentel@ipca.pt; pedrofrcosta@gmail.com; jvilaca@ipca.pt; cmscosta@fisica.uminho.pt; lanceros@fisica.uminho.pt; damiranda@ipca.pt

Abstract. Nowadays is a constant demand for new and/or improved health treatments that uses flexible sensor devices. One in particular is the neurogenic bladder dysfunction. Normally the polymeric materials used in this treatments are synthetic what can be a problem because today exist a constant demand for natural materials that don't harm and that have a reduce impact on the environment. In this context was produced a comparison between polymer composites on three different matrices, carboxymethyl cellulose (CMC), styrene-ethylene/butylene-styrene (SEBS) and polyvinyl alcohol (PVA), with different concentrations of multi-walled carbon-nanotubes (CNT) filler contents for catheter medical device application. Furthermore, the functional performance of the composites were characterized by the piezoresistive response. Finally, a proof-of-concept, based on a PVA composite was elaborated. In the end was proved that the screen-printable piezoresistive sustainable composites can be developed for a medical device application.

Keywords: piezoresistive sensors· printing techniques· medical devices.

1 Introduction

In some persons the urine flows from the bladder back into the ureters this is called Vesicoureteral reflux. When this happens kidney damage can occur [1]. The treatment used today focuses mainly on medications or in a specific procedure called clean intermittent catheterization (CIC) and the process is carried out via insertion of a urinary catheter into the urethra to remove the urine. This is a very difficult task that can lead to injuries for the patient . [2]. The development of novel solutions is of the most urgent importance. A possible arrangement to avoid these type of undesirable complications can be the implementation of sensors that measures the strength and deformation and monitor the route along the urethra represents a real need. Piezoresistive sensors appear to be a suitable solution due to their electrical conductivity variations under mechanical deformation with high sensitivity, simple working principle, low energy consumption, high sensing range for a long and stable period of time, and low cost when compared

to other types of sensors. The most interesting are the polymer composites based on a polymeric matrix and conductive fillers. Thus, different synthetic polymers, such as styrene-ethylene/butylene-styrene (SEBS) and silicon were already introduced for the development of sensors for biomedical devices These polymers present some ecological disadvantageous, including the use of non-renewable materials and the need of hazard solvents during processing, so a possible solution is the substitution by natural polymers, which are biocompatible, biodegradable, and some of them are processable with environmental friendly solvents. [3]. The aim of this work is to create different polymers (SEBS,CMC and PVA) varying the conductive filler content to produced piezoresistive sensors that can be implemented in a biomedical device.

2 Experiments and Results

First the selected polymers (SEBS,CMC and PVA) and the corresponding composites were prepared with different % 0, 1, 2, 3, 4 and 5 weight percentage (wt. %) of CNT by the method of solvent casting. In order to select the most suitable sample to printed in the catheter, a proper evaluation was executed to determine the electrical and mechanical properties as seen in figure 1a) and b) .

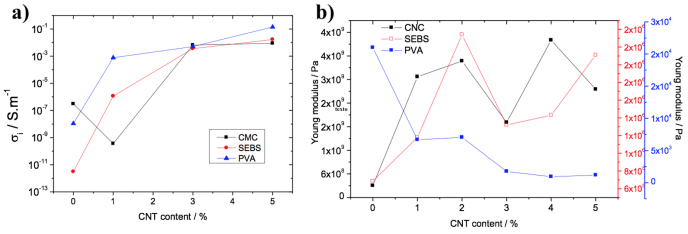

Fig. 1: a)- Electrical conductivity of the PVA, CMC, and SEBS polymer composites as a function of the % CNTs b)Tensile stress-strain mechanical curves for CMC and PVA of the different composites. .

In accordance with figure 1 is possible to identified that all polymers present electrical conductivity from 3% CNT content and that the mechanical proprieties in PVA samples are improved in relation to the CMC samples. Having these in consideration the PVA samples were selected due to the suitable proprieties and the use of a natural solvent. This one was then printed by a screen printing method as seen in figure 2 a). In the end was realized an piezoresistive test as seen in figue 2 b) that demonstrate that has an gauge factor of 1,6 for a deformation of 3mm.

Acknowledgments

The authors thank the Fundação para a Ciência e Tecnologia for financial support under framework of the Strategic Funding UIDB/05549/2020, UIDP/05549/2020, LASI-LA/P/0104/2020, UIDB/04650/2020, UID/FIS/04650/2021 and UIDB/00319/2020 and project SmartHealth, "NORTE-01-0145- FEDER-000045", supported by Northern Portugal Regional Operational Programme (Norte2020), under the Portugal 2020 Partnership Agreement, through the European Regional Development Fund (ERDF). The authors also thank the FCT for financial support under individual research grant UI/BD/151058/2021 (E.P.), grant SFRH/BPD/110914/2015 (P.C.) and FCT investigator contract 2020. 04028.

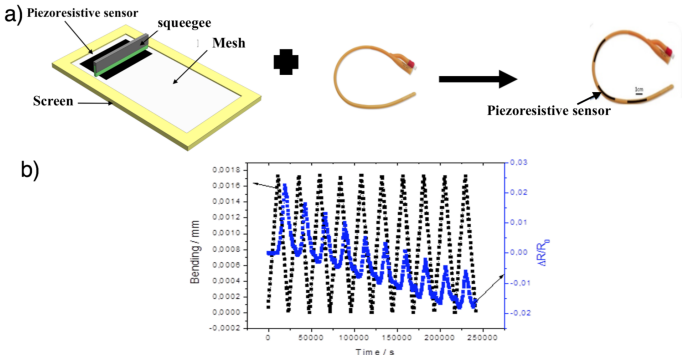

Fig. 2: a)Schematic representation of the screen-printing method used to print the piezoresistive sensors in the urinary catheter. b)Bending piezoresistive performance of the PVA piezoresistive sensors with 3%CNTs

References

1. Elder, J.S. et al., Pediatric Vesicoureteral Reflux Guidelines Panel summary report on the management of primary vesicoureteral reflux in children. The Journal of urology. *The Journal of urology*, 1997.
2. V.P. Alencar. Impact of the route of clean intermittent catheterization on quality of life in children with lower urinary tract dysfunction. *Neurourology and Urodynamics, 2018.*
3. *Gowthaman, N. et al. Advantages of biopolymers over synthetic polymers: social, economic, and environmental aspects, in Biopolymers and their Industrial Applications.* Elsevier*, 2021.*

Classification of Continuous ECG Segments - Performance Analysis of a Deep Learning Model

Luís C. N. Barbosa[1], Diogo Lopes[1], Inês Escrivães[1], António H. J. Moreira[1], Vítor Carvalho[1], João L. Vilaça[1], and Pedro Morais[1]

Instituto Politécnico do Cávado e do Ave, IPCA, Portugal
lbarbosa@ipca.pt, dlopes@ipca.pt, iescrivaes@ipca.pt, amoreira@ipca.pt, vcarvalho@ipca.pt, jvilaca@ipca.pt, pmorais@ipca.pt

Abstract. Classification of electrocardiogram (ECG) signals plays an important role in diagnosing heart diseases. It is a complex and non-linear signal, which is the first option to preliminary identify specific pathologies/conditions (e.g., arrhythmias) [1]. Currently, the scientific community has proposed a multitude of intelligent systems to automatically process the ECG signal, through deep learning techniques, as well as machine learning, where this present high performance, showing state-of-the-art results [2]. However, most of these models are designed to analyze the ECG signal individually, i.e., segment by segment [3].
The scientific community states that to diagnose a pathology in the ECG signal, it is not enough to analyze a signal segment corresponding to the cardiac cycle, but rather an analysis of successive segments of cardiac cycles, to identify a pathological pattern [4] [5].
In this paper, an intelligent method based on a Convolutional Neural Network 1D paired with a Multilayer Perceptron (CNN 1D+MLP) [6] was evaluated to automatically diagnose a set of pathological conditions, from the analysis of the individual segment of the cardiac cycle. In particular, we intend to study the robustness of the referred method in the analysis of several simultaneous ECG signal segments. Two ECG signal databases were selected, namely: MIT-BIH Arrhythmia Database (D1) and European ST-T Database (D2) [7]. The data was processed to create datasets with two, three and five successive segments in a row, to train and test the performance of the method (Fig.1). The method was evaluated in terms of classification metrics, such as precision, recall, f1-score, and accuracy, as well as through the calculation of confusion matrices.
Overall, the method demonstrated high robustness in the analysis of successive ECG signal segments, which we can conclude that it has the potential to detect anomalous patterns in the ECG signal. In the future, we will use this method to analyze the ECG signal coming in real-time, acquired by a wearable device, through a cloud system.

Keywords: Deep Learning; · ECG Classification; · ECG Databases; · Artificial Intelligence; · Wearable Device.

1 Introduction

Currently, several researchers propose studies that use AI, namely through deep learning and machine learning techniques for the detection and classification of arrhythmias, through the analysis of the ECG signal. However, due to the fact that the ECG signal is recurrent in nature, the analysis of this signal is often based on samples extracted from the same location of segments from different periods of the signal. Thus, an abnormal sporadic event in a cardiac segment does not definitively confirm that the patient has some type of arrhythmia, as each type of cardiac pathology temporarily or affects permanently, totally or partially, the basic waveform of the ECG. In this sense, an abnormal sporadic event in a cardiac segment does not definitively confirm that the patient has some type of arrhythmia. Therefore, the general idea of this study is to evaluate the performance of a state-of-the-art AI method, training the model to classify two, three or five successively segments of the ECG signal, and verify if the performance of the method changes. With such strategy, we aim to study if the inclusion of temporal information in the training of the AI leads to an improvement in the classification process.

2 Databases

Two databases were selected for this study: MIT-BIH Arrhythmia Database (D1) and European ST-T Database (D2). The choice of these is due to a second study developed by us, where a literature review was carried out by public ECG signal databases [7]. Only similar classes between the two databases were selected for the study, as described in Table 1.

Table 1: Datasets Description.

Category	Description	Segments (D1/D2)
N	Normal Beat	90631 / 784633
S	Supraventricular Premature Beat	2781 / 1095
V	Premature Ventricular Contraction	7236 / 4467
F	Fusion of Ventricular and Normal Beat	803 / 354
Q	Unclassifiable Beat	8043 / 8054

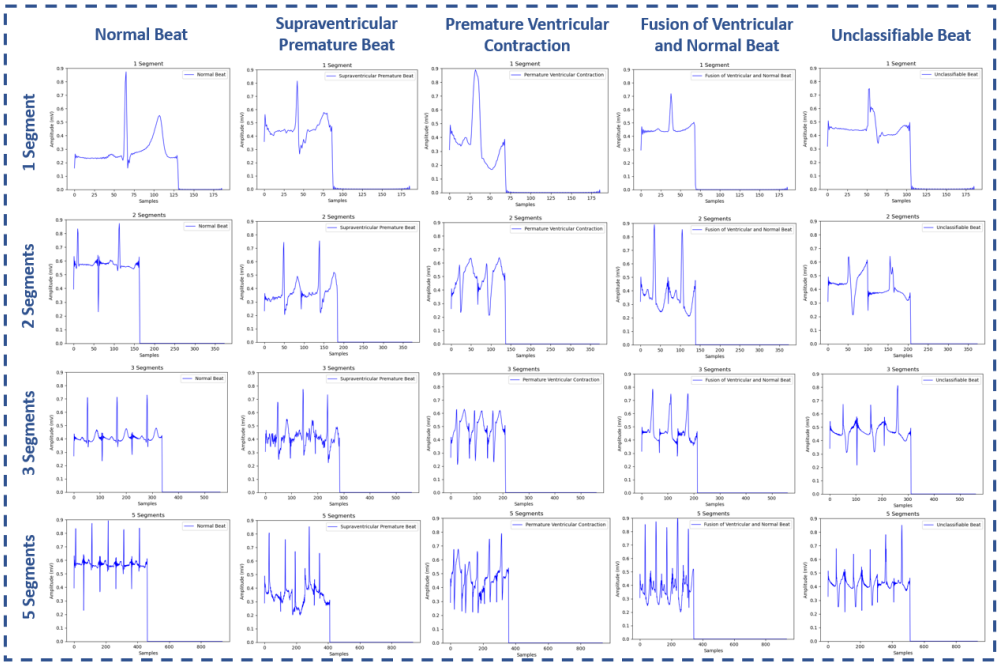

Fig. 1: Waveforms of different sets of ECG signal segments in different classes.

3 ECG Classifier

This method used a 1D Convolutional Network paired with a Multilayer Perceptron (MLP). The proposed technique relies on five blocks, namely: four initial blocks of convolutional operations and a final MLP. The reason why this architecture was chosen was that it showed greater robustness in the study carried out in [3].

4 Conclusion

This study suggested that heartbeat classification based on the CNN1D+MLP architecture is robust in classifying one cardiac segment, or successive cardiac segments (two, three, or five). This allows us to conclude that this method is a tool with the potential to detect anomalous patterns along the ECG signal because a pathological condition is not only visible in one cardiac segment, but in multiples.

Acknowledgment

This project was funded by the projects "NORTE-01-0145-FEDER-000045", supported by Northern Portugal Regional Operational Programme (Norte2020), and NORTE-01-0247- FEDER-070200, supported by COMPETE - Competitiveness and Internationalization Operational Program (COMPETE 2020), under the Portugal 2020 Partnership Agreement, through the European Regional Development Fund (ERDF). It was also financed by national funds, through FCT - Foundation for Science and Technology and FCT / MCTES under the project UIDB / 05549/2020, UIDP/05549/2020, CEECINST/00039/2021 and LASI-LA/P/0104/2020. This project was also funded by the Innovation Pact HfFP – Health From Portugal, co-funded from the "Mobilizing Agendas for Business Innovation" of the "Next Generation EU" program of Component 5 of the Recovery and Resilience Plan (RRP), concerning "Capitalization and Business Innovation", under the Regulation of the Incentive System "Agendas for Business Innovation".

References

1. Muhammad Wasimuddin, Khaled Elleithy, Abdel-Shakour Abuzneid, Miad Faezipour, Omar Abuzaghleh. Stages-Based ECG Signal Analysis From Traditional Signal Processing to Machine Learning Approaches : A Survey. *IEEE Access*, 8, 2020.
2. Ulas Baran Baloglu, Muhammed Talo, Ozal Yildirim, Ru San Tan, and U. Rajendra Acharya. Classification of myocardial infarction with multi-lead ECG signals and deep CNN. *Pattern Recognition Letters*, 122:23–30, may 2019.
3. Luís C N Barbosa, António Real, António H J Moreira, Vítor Carvalho, João L Vilaça, and Pedro Morais. EGG Classification with Deep Learning Models – A Comparative Study. pages 9–12, 2020.
4. Francisco Castells, Pablo Laguna, Leif Sörnmo, Andreas Bollmann, and José Millet Roig. Principal component analysis in ECG signal processing. *Eurasip Journal on Advances in Signal Processing*, 2007, 2007.
5. Rosaria Silipo and Carlo Marchesi. Artificial neural networks for automatic ECG analysis. *Society*, 46(5):1417–1425, 1998.
6. Ines Escrivaes, Luis C.N. Barbosa, Helena R. Torres, Bruno Oliveira, Joao L. Vilaca, and Pedro Morais. ECG classification using Artificial Intelligence: Model Optimization and Robustness Assessment. *SeGAH 2022 - 2022 IEEE 10th International Conference on Serious Games and Applications for Health*, 2022.
7. Biosignal Databases for Training of Artificial Intelligent Systems. *ACM International Conference Proceeding Series*, pages 74–81, sep 2022.

Modeling the COVID-19 post-pandemic spread

Carlos Balsa[1,2], Everaldo Junior Borges Garcia de Padua[3], Luan Crisostomo Pinto[3], and José Rufino[1,2]

[1] Research Centre in Digitalization and Intelligent Robotics (CeDRI), Instituto Politécnico de Bragança, Campus de Santa Apolónia, 5300-253 Bragança, Portugal
{balsa,rufino}@ipb.pt
[2] Laboratório para a Sustentabilidade e Tecnologia em Regiões de Montanha (SusTEC), Instituto Politécnico de Bragança, Campus de Santa Apolónia, 5300-253 Bragança, Portugal
[3] Instituto Politécnico de Bragança, Portugal
{a57328,a57329}@alunos.ipb.pt

Abstract. With the current recession of the global COVID-19 pandemic, the corresponding epidemic models need to be adapted to reflect this new reality and continue assisting public health authorities in the definition of policies and decision making. With that aim, this paper presents a deterministic SEIR epidemic model for the representation of the COVID-19 post-pandemic scenario. The model considers the effect of countermeasures such as vaccination and quarantine, and the consequences of the progressive loss of immunity. The preliminary evaluation results, with fixed parameters, point to a cyclic evolution of the pandemic and a tendency for stabilization in the future.

Keywords: COVID-19 · post-pandemic scenario · SEIR model.

1 Introduction

The present work focuses on the dynamics of COVID-19 spreading in a post-pandemic scenario, in which a large part of the population is regularly vaccinated. Thus, a new epidemic mathematical model is proposed, adapted to a post-pandemic situation, considering not only the control measures represented by vaccination and isolation but also the effects of the loss of immunity of infected and vaccinated individuals. A new compartmental model, SEIRVQD (for Susceptible, Exposed, Infected, Recovered, Vaccinated, Quarantined, and Deceased), was developed. Based on that, a deterministic formulation was created, these dynamics are represented by the System of (differential) Equations (1):

$$\begin{cases} \frac{\partial S}{\partial t} = \omega_V V + \sigma_R R - \psi_V S - \frac{\beta I}{N} S \\ \frac{\partial E}{\partial t} = \frac{\beta I}{N}(S + (1-\varepsilon)\,V) - \tau_E E \\ \frac{\partial I}{\partial t} = \tau_E E - \alpha_S\,(1-\gamma)\,I - \gamma I \\ \frac{\partial R}{\partial t} = \alpha_S\,(1-\theta-\gamma)\,I + \alpha_Q(1-\theta)Q - \sigma_R R \\ \frac{\partial D}{\partial t} = \theta\alpha_S I + \theta\alpha_Q Q \\ \frac{\partial V}{\partial t} = \psi_V S - \frac{\beta I}{N}\,(1-\varepsilon)\,V - \omega_V V \\ \frac{\partial Q}{\partial t} = \gamma I \alpha_Q Q \end{cases} \tag{1}$$

Each equation describes the evolution of the number of individuals in each state (compartment) on day t, with $S(t)$=susceptibles, $E(t)$= exposed to the disease but not

infectious, $I(t)$=infected, $R(t)$=recovered from the disease and now immune, $D(t)$=died from the disease, $V(t)$=vaccinated and $Q(t)$=quarantined.

The constants ψ_V, ω_V, β, ϵ, τ_E, α_S, γ, θ, α_Q and σ_R are the parameters of the model. Its values are crucial in determining the outcome of the simulations, as they define how the pandemic events occur [1].

The method used to define the vaccination rate (ψ_V) and the mortality rate (θ), was a simple linear regression, from the cumulative values available in the dataset [2]. The analysis interval is from January 1 to March 24, 2023. The data refer to Portugal and are the most up-to-date at the time of this study.

The quarantine rates, γ and α_Q, were arbitrarily defined, once they have currently no meaningful impact due to the low number of infected people.For the transmission rate (β), a reliable value was calculated based on the reproduction number R(t) reports [3]. The vaccine protection rate (ω_V), the efficacy of the vaccine (ϵ), the average latency period (τ_E), the recovered or deceased rate (α_S) and the rate of loss of natural immunity (σ_R) were collected by a literature research. All constants and corresponding references can be found in Table 1.

Table 1: Values of the SEIRVQD Model Parameters.

Symbol	**Value**	**Description**	**Reference**
ψ_V	0.00018559	Vaccination rate	[2]
ω_V	1/180	Vaccine decline rate	[4]
β	[0.1854-0.1945]	Transmission contact rate	[3]
ε	[0.903-0.976]	Vaccine efficiency	[4]
τ_E	[0.1695-0.1961]	Average latency period	[5]
α_S	0.0925069	Transition rate for recovered or deceased	[4]
γ	0.025	Quarantine rate	Arbitrary
θ	0.0000006555	Fraction of individuals who die from the disease	[2]
α_Q	[0 - 1/5]	Rate of quarantined who recovered or died	Arbitrary
σ_R	1/240	Natural immunity loss rate	[6]

2 Results

The evolution of the number of individuals in each compartment of a population with N=100000 individuals, generated by the deterministic System of Equations (1), over 1500 days, is shown in Fig. 1. The results were obtained through the numerical resolution of the initial value problem given by that system of equations with initial conditions $S(0)$=1999, $E(0)$=0, $I(0)$=1, $V(0)$=98000, $Q(0)$=0, $D(0)$=0 and $R(0)$=0. The system was solved using the built-in MATLAB function `ode45`, which combines the 4th and 5th-order Runge-Kutta methods.

It is possible to observe waves in the evolution of the number of susceptible individuals and recovered ones, as well as a decrease in the vaccinated population. The model also describes the possibility of small infectious outbreaks with decreasing magnitude. This provides motivation to pursue the study of the evolution of the spread of the COVID-19 disease in a post-pandemic scenario.

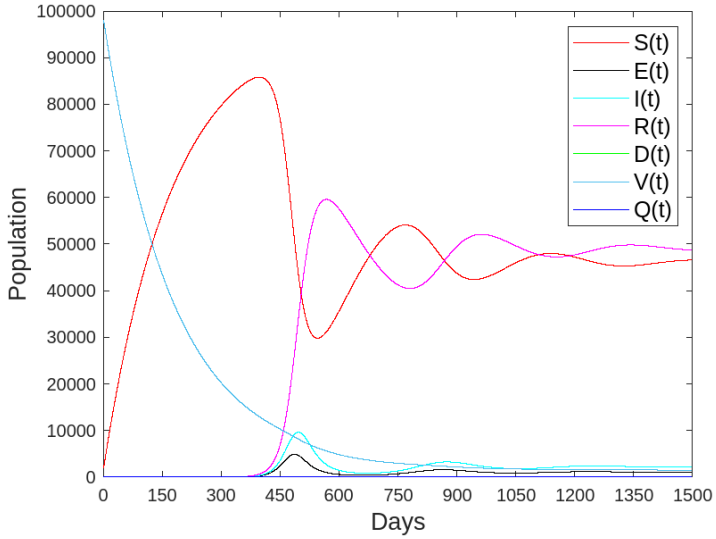

Fig. 1: Simulation Results of the SEIRVQD Deterministic Model.

To conclude, the model proposed is adapted to the specifics of a post-pandemic regime, by accounting for the effect of vaccination and loss of immunity. Furthermore, even though the model was created keeping in mind the COVID-19 pandemic, it can be easily adapted to the spread of other infectious diseases.

References

1. Herbert W. Hethcote. The mathematics of infectious diseases. *SIAM Review*, 42(4):599–653, 2000.
2. Edouard Mathieu, Hannah Ritchie, Lucas Rodés-Guirao, Cameron Appel, Charlie Giattino, Joe Hasell, Bobbie Macdonald, Saloni Dattani, Diana Beltekian, Esteban Ortiz-Ospina, and Max Roser. Coronavirus pandemic (covid-19). *Our World in Data*, 2020. https://ourworldindata.org/coronavirus.
3. Baltazar Nunes, Constantino Caetano, Liliana Antunes, Susana Silva, Ausenda Machado, Ana Rodrigues, Carlos Dias, and Luísa Morgado. Evolução do número de casos de covid-19 em portugal. *Instituto Nacional de Saúde*, April 2023.
4. Manuel Adrian Acuña-Zegarra, Saúl Díaz-Infante, David Baca-Carrasco, and Daniel Olmos-Liceaga. Covid-19 optimal vaccination policies: A modeling study on efficacy, natural and vaccine-induced immunity responses. *Mathematical Biosciences*, 337:108614, 2021.
5. Hualei Xin, Yu Li, Peng Wu, Zhili Li, Eric H Y Lau, Ying Qin, Liping Wang, Benjamin J Cowling, Tim K Tsang, and Zhongjie Li. Estimating the latent period of coronavirus disease 2019 (covid-19). *Clinical Infectious Diseases*, 74(9):1678–1681, 09 2021.
6. João Malato, Ruy M Ribeiro, Eugénia Fernandes, Pedro Pinto Leite, Pedro Casaca, Carlos Antunes, Válter R Fonseca, Manuel Carmo Gomes, and Luis Graca. Stability of hybrid versus vaccine immunity against ba.5 infection over 8 months. *The Lancet Infectious Diseases*, 23(2):148–150, 2023.

CycleGAN-Based Image to Image Translation for Realistic Surgical Training Phantoms

N. S. Rodrigues[1,2,3], H. Torres[1,2,3,4], P. Morais[1,3], L. R. Buschle[5], S. Haag[5], J. Correia-Pinto[2], E. Lima[2], and J. L. Vilaça[1,3]

[1] 2Ai – School of Technology, IPCA, Barcelos, Portugal
[2] Life and Health Sciences Research Institute (ICVS), School of Medicine, University of Minho, Braga, Portugal
[3] LASI - Associate LAboratory of Intelligent Systems, Guimarães, Portugal
[4] Algoritmi Center, School of Engeneering, University of Minho, Guimarães, Portugal
[5] Karl Storz SE Co. KG, Tuttlingen, Germany
ndrodrigues@ipca.pt

Abstract. Training in surgery is essential for surgeons to develop skill and dexterity [1]. Physical training phantoms provide excellent haptic feedback and tissue properties for stitching and operating with authentic instruments and are easily available. However, they lack realistic traits and fail to reflect the complex environment of a surgical scene [2], [3]. Generative Adversarial Networks can be used for image-to-image (I2I) translation, addressing the lack of realism in physical phantoms, by mapping patterns from the intraoperative domain onto the video stream captured during training with these surgical simulators [4]. This work aims to achieve a successful I2I translation, from intra-operatory mitral valve surgery images onto a surgical simulator, using the CycleGAN model. Different experiments are performed - comparing the Mean Square Error Loss with the Binary Cross Entropy Loss; validating the Fréchet Inception Distance as a training and image quality metric; and studying the impact of input variability on the model performance. Differences between MSE and BCE are modest, with MSE being marginally more robust. The FID score proves to be very useful in identifying the best training epochs for the CycleGAN I2I translation architecture. Carefully selecting the input images can have a great impact in the end results. Using less style variability and input images with good feature details and clearly defined characteristics enables the network to achieve better results.

Keywords: CycleGAN · Surgical Phantoms · Minimally Invasive Surgery.

1 Methodology and Results

For the I2I translation task we implemented the CycleGAN model proposed by [5], which aims at obtaining mapping functions between two different domains (A and B), without the need for paired images in the input (Unsupervised I2I translation). The AdaptOR challenge dataset was used. The cohort splits into two endoscopic sets with data acquired during mitral valve repair training on a surgical simulator ("Sim Domain") and intraoperative endoscopic data from real minimally invasive mitral valve repair ("Intra-op Domain") [6]. To develop our methods, data were split to create a validation set, isolating images from 3 simulations and 1 Intra-op procedure, corresponding to a Training-Validation ratio of approximately 70:30. The validation dataset is used to evaluate our training and choose the best training epoch.

The model was trained with the original RGB images, with a 512 x 288 resolution, varying only the loss function for the Generator and Discriminator networks, over 80 epochs, with a batchsize of 1 and a learning rate of 0.0001, linearly decaying to 0

after the 40th epoch. For the Generator and Discriminator networks, two different loss functions were implemented and compared: 1) Mean Squared Error (MSE); 2) Binary Cross Entropy with logits (BCE). For both Cycle and Identity losses, the L1 norm was used. Evaluation was performed on the validation dataset, taking only into account the fake intra-op images, since that was the goal of this work – generate realistic images from a synthetic training phantom. FID score was used to compare the fake intra-op images, for both trainings (MSE and BCE). FID scores were obtained by comparing the generated images, for each epoch, against the set of images from the training dataset, to have a fair correlation of features and surgical style distribution. Finally, an additional training was conducted, for both losses, with a single surgical style to evaluate the GAN behavior when trained with less input variability. Surgical style 3 was chosen, as initial experiments showed indication of this style providing a more reliable feature input to the Generator network. A sample of the results obtained with the previously described experiments is shown in Figure 1.

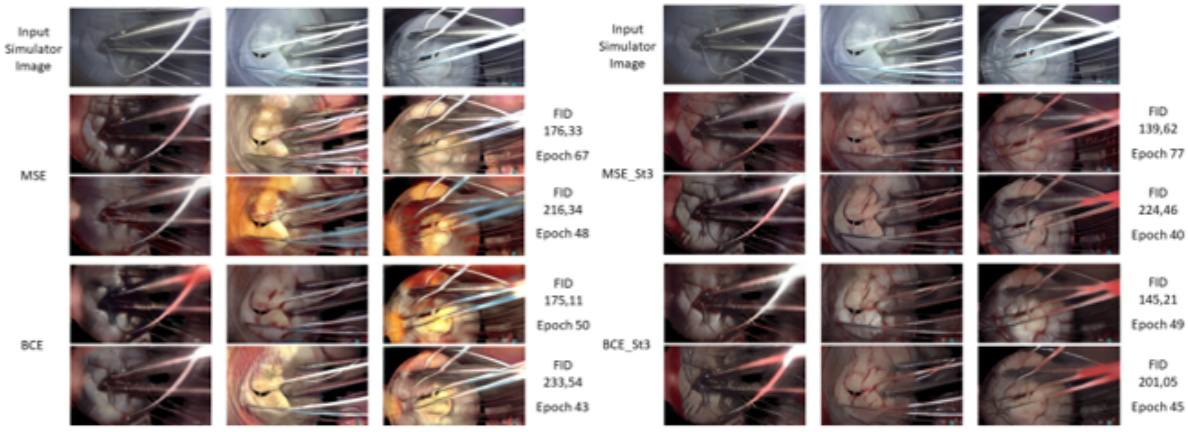

(a) All surgical styles as input.

(b) Only surgical style 3 as input.

Fig. 1: Obtained results for both training losses with all surgical styles and only surgical 3 as input. Top row: original phantom image. 2nd and 3rd rows: best and worst FID scores for MSE, respectively. 4th and 5th rows: best and worst FID scores for BCE, respectively.

Although not drastically, generally, MSE is more stable than BCE, and achieves acceptable results in a fewer number of epochs. A lower FID score successfully indicates a better set of generated images showing potential for a more objective selection of the best training epochs. Carefully selecting the input is crucial to condition how the network performs.

Acknowledgements

The authors acknowledge the company KARL STORZ SE Co. KG for their support of this research. This project was funded by the projects "NORTE-01-0145-FEDER-000045", "NORTE-01-0145-FEDER-000055" and "NORTE-01-0145-FEDER-000059",

supported by Northern Portugal Regional Operational Programme (Norte2020), under the Portugal 2020 Partnership Agreement, through the European Regional Development Fund (ERDF). It was also financed by national funds, through FCT - Foundation for Science and Technology and FCT / MCTES under the project UIDB / 05549/2020, UIDP/05549/2020, UIDB/50026/2020, UIDP/50026/2020, CEECINST/00039/2021 and LASI-LA/P/0104/2020. This project was also funded by the Innovation Pact HfFP – Health from Portugal, co-funded from the "Mobilizing Agendas for Business Innovation" of the "Next Generation EU" program of Component 5 of the Recovery and Resilience Plan (RRP), concerning "Capitalization and Business Innovation", under the Regulation of the Incentive System "Agendas for Business Innovation". The authors also acknowledge FCT, Portugal and the European Social Fund, European Union, for funding support through the "Programa Operacional Capital Humano" (POCH) in the scope of the PhD grant SFRH/BD/136670 (H.R. Torres).

References

1. Chung, R.S.: How much time do surgical residents need to learn operative surgery? American Journal of Surgery **190**, 351–353 (2005). https://doi.org/10.1016/j.amjsurg.2005.06.035
2. Belenchon, I.R., Ruiz, C.B.C., Ciriza, G.G., Santos, V.G.D., Asensio, C., Gordaliza, C.G., Garcia, I.O., Sanchez, J.M.C., Revilla, F.J.B., Lopez, R.A.M.: Mp41-19 phase i nct03738488. feasible 3d printed models of renal cell carcinoma with venous thrombus extension for surgical planning and simulation. Journal of Urology **207**, 728–729 (2022). https://doi.org/10.1097/ju.0000000000002607.19
3. Engelhardt, S., Sauerzapf, S., Al-Maisary, S., Karck, M., Preim, B., Wolf, I., Simone, R.D.: Elastic mitral valve silicone replica made from 3d printable molds offer advanced surgical training. Informatik aktuell **c**, 74–79 (2018).
4. Pang, Y., Lin, J., Qin, T., Chen, Z.: Image-to-image translation: Methods and applications. IEEE Transactions on Multimedia **24**, 3859–3881 (2022). https://doi.org/10.1109/TMM.2021.3109419
5. Zhu, J.Y., Park, T., Isola, P., Efros, A.A.: Unpaired image-to-image translation using cycle-consistent adversarial networks. Proceedings of the IEEE International Conference on Computer Vision **2017-Octob**, 2242–2251 (2017). https://doi.org/10.1109/ICCV.2017.244
6. Sharan, L., Romano, G., Koehler, S., Kelm, H., Karck, M., Simone, R.D., Engelhardt, S.: Mutually improved endoscopic image synthesis and landmark detection in unpaired image-to-image translation. IEEE Journal of Biomedical and Health Informatics **26**, 127–138 (2022). https://doi.org/10.1109/JBHI.2021.3099858

Simulated Waste Fulfilling to Assess the Performance of Ultrasonic Sensors in Measuring Waste Levels*

Adriano Silva[1,2,3,4,5], João Mendes[1,3], Thadeu Brito[1,3], José Lima[1,3], Ana I. Pereira[1,3], Adrián M. T. Silva[3,4], and Helder T. Gomes[2,3]

[1] Research Centre in Digitalization and Intelligent Robotics (CeDRI), Instituto Politécnico de Bragança, 5300-253 Bragança, Portugal
{adriano.santossilva, joaocmendes, brito, apereira,jllima,htgomes}@ipb.pt
[2] Centro de Investigação de Montanha (CIMO), Instituto Politécnico de Bragança, 5300-253 Bragança, Portugal
htgomes@ipb.pt
[3] Laboratório Associado para a Sustentabilidade e Tecnologia em Regiões de Montanha (SusTEC), Instituto Politécnico de Bragança, 5300-253 Bragança, Portugal
[4] Laboratory of Separation and Reaction Engineering – Laboratory of Catalysis and Materials (LSRE-LCM), Faculty of Engineering, University of Porto, Porto, Portugal
[5] ALiCE - Associate Laboratory in Chemical Engineering, Faculty of Engineering, University of Porto, Portugal
adrian@fe.up.pt

Abstract. The rapid growth of urban informatization through Information and Communication Technologies (ICT) has propelled the development of smart cities, leveraging technology integration to enhance services and infrastructure across sectors. Waste collection in smart cities has shifted towards data-driven route optimization, using powerful analytics and sensor networks. While these approaches rely on computational techniques and data, accurately measuring waste generation remains challenging. An emerging solution involves wireless sensor networks to monitor real-time waste levels inside dumpsters, improving efficiency and reducing costs. This study focuses on assessing the accuracy of IoT sensor systems for waste level measurement, demonstrating reliable results. This research supports using such systems for enhancing waste management in smart cities.

Keywords: Waste level · Physical measurement · IoT.

1 Introduction

Recent waste collection efforts in smart cities have targeted route optimization [1]. Various methodologies, such as data analytics, have optimised different aspects of waste collection, including waste prediction, cyber-physical route scheduling, and bin mapping. While these approaches rely solely on computational techniques and do not necessitate physical infrastructure changes, they rely highly on data from the relevant waste management authorities. The stochastic nature of waste generation still poses challenges for precise route scheduling, resulting in issues like visiting empty dumpsters and bins overflowing due to delayed collection. Similarly, Rizvanoglu et al. applied linear

* This work has been supported by FCT - Fundação para a Ciência e Tecnologia within the R&D Units Project Scope: UIDB/05757/2020, UIDP/05757/2020, UIDB/00690/2020, UIDB/50 020/2020, and UIDB/00319/2020. Adriano Silva was supported by FCT-MIT Portugal PhD grant SFRH/BD/151346/2021, and Thadeu Brito was supported by FCT PhD grant SFRH/BD/08598/2020. The authors are grateful to Sociedade Ponto Verde for the finantial support through the project "A digitaização como ferramenta para melhorar a sustentabilidade do processo de recolha seletiva".

programming and geographic information systems (GIS) to enhance routes, achieving substantial savings of up to 33% [2].

In recent years, another approach has been raising attention due to the good results obtained in study cases developed worldwide. This approach uses a wireless sensor network to collect real-time data regarding waste levels inside dumpsters [3]. This information is then stored in the cloud and used to support decision-making on the need for collection and route planning for the collection task. Each study considers its own set of sensors for measurement and IoT protocol for communicating levels to the cloud. Despite each physical system's structure, most consider parameters such as distance, temperature, humidity and load to measure waste level inside dumpsters. Oralhan *et al.* developed one prototype for smart waste management that can measure waste level, the temperature inside the dumpster, and the ratio of carbon dioxide inside the container [4]. All these parameters are then sent to the cloud using IoT technology, and route optimization for collection is performed using an ant colony optimization algorithm. Moreover, data mining is used to forecast when dumpsters will reach the maximum waste level, another information useful for waste collection planning. Their approach was applied in 200 waste containers in Kayseri (Turkey), returning about 30% in waste collection cost savings.

2 Methodology

Despite the high number of studies dealing with waste collection optimization via IoT technology, most works fail to present the accuracy of their system for measuring waste levels inside dumpsters. For this reason, the present study will show the results obtained for measuring waste levels inside a simulated dumpster using a system of sensors described in more detail in a previous work [5]. In brief, the system comprises an ultrasonic sensor HC-SR04 and a humidity and temperature sensor DHT11, allowing to determine with high accuracy the distances from solid objects regardless of the temperature and humidity of the environment. The set of sensors was connected to an ESP32 to send information on waste levels inside dumpsters directly to the cloud, with an interval of 10 seconds. Plastic waste was introduced inside the simulated dumpster at periodic times to determine the capacity of the set to measure the waste levels inside dumpsters. For this, 10% of the model waste was added into the dumpster, followed by a period of 1 minute without the addition of waste. The same procedure was repeated until using the complete amount of waste (70 water bottles of 1.5 L). The fulfilling experiment was performed three times following the same procedure described above.

3 Results

The results demonstrate that each waste addition was responsible for changing the waste level by 8%, which achieved a maximum waste level of around 80%. The level measured during the addition of waste inside the dumpster returned measured waste levels that represent around 5% of error, which would not severely impact the future application of decision-making for route planning based on waste levels. The measurements for periods in which no waste was added returned stable values for all runs performed, with

oscillations lower than 1%. This result demonstrated that the set of sensors considered for this application could return stable waste level measurement, which was a concern regarding using ultrasonic sensors for this application. The experiment performed in these conditions revealed the potential feasibility of this solution for further assembly of wireless sensors network to measure waste levels inside dumpsters and support waste collection optimization routes. For instance, in future studies, the waste set will be increased to reach the full capacity of the dumpster, and tests will be performed with more waste types from different sources. Furthermore, experiments using wet waste will also be performed to determine if this parameter influences waste level measurement using ultrasonic sensors.

References

1. María-Victoria Bueno-Delgado, Pilar Romero-Gázquez, and Pablo Pavón-Mariño. Optimal path planning for selective waste collection in smart cities. *Sensors*, 19(9):1973, 2019.
2. Onur Rızvanoğlu, Serkan Kaya, Mustafa Ulukavak, and Mehmet İrfan Yeşilnacar. Optimization of municipal solid waste collection and transportation routes, through linear programming and geographic information system: a case study from şanlıurfa, turkey. *Environmental Monitoring and Assessment*, 192:1–12, 2020.
3. Theodoros Anagnostopoulos, Arkady Zaslavsky, Stefanos Georgiou, and Sergey Khoruzhnikov. High capacity trucks serving as mobile depots for waste collection in iot-enabled smart cities. In *Internet of Things, Smart Spaces, and Next Generation Networks and Systems: 15th International Conference, NEW2AN 2015, and 8th Conference, ruSMART 2015, St. Petersburg, Russia, August 26-28, 2015, Proceedings 15*, pages 80–94. Springer, 2015.
4. Zeki Oralhan, Burcu Oralhan, and Yavuz Yiğit. Smart city application: Internet of things (iot) technologies based smart waste collection using data mining approach and ant colony optimization. *Internet Things*, 14(4):5, 2017.
5. Adriano S Silva, Thadeu Brito, Jose L Diaz de Tuesta, José Lima, Ana I Pereira, Adrián MT Silva, and Helder T Gomes. Node assembly for waste level measurement: Embrace the smart city. In *Optimization, Learning Algorithms and Applications: Second International Conference, OL2A 2022, Póvoa de Varzim, Portugal, October 24-25, 2022, Proceedings*, pages 604–619. Springer, 2023.

Robotic Tools for Upper Limb Rehab: A kinematic Study

Joaquin Dillen[1], Antonio Moreira[1], and João Vilaça[1]

2Ai - Instituto Politécnico do Cávado e do Ave, Portugal
{jdillen, amoreira, jvilaca}@ipca.pt

Abstract. The study aims to analyze the kinematics of a robotic arm with a tool for upper limb rehabilitation, with a focus on implementing the necessary hardware and software to enable the addition of rehabilitation tools to the robotic arm similar work is being developed in ROBERT®, BURT® and ArmMotus™ EMU. The mechanical parameters of the robotic arm design for rehabilitation purposes, including dimensions, weights, and angles, are analyzed. The kinematic model is determined by analyzing the different frames of the axis, followed by the determination of the dynamic model for each joint using simulation software. V-REP is used for simulation and 3D analysis. The results will be a Denavit-Hartenberg table that can be used for further analysis of the kinematics of the solution, including precision, stability, and strength the advantages of this information will help to have a clearer mathematical understanding of the solution which will lead to an enhanced way of operability. The proposed approach will assist physicians in treating multiple patients simultaneously, increasing efficiency and productivity in the healthcare sector.

Keywords: Kinematic model · simulation · kinematics · Denavit-Hartenberg · Upper-limb Rehabilitation.

1 Introduction

1.1 KUKA LBR iiwa 7 R800

This article analyzes the addition of an upper limb rehabilitation [1] [2] tool to the LBR iiwa 7 R800, a medical-grade robotic arm with well-studied kinematics [3]. Precise movement trajectories of the rehabilitation tool are crucial for upper-limb rehabilitation in patients. The robotic arm must be versatile, able to dynamically manage different joints, converge the exercise requirements, as well as individual patient differences. A careful study and dynamic regime are necessary to simulate different behaviors and ensure patient safety in our proposed solution.

1.2 Rehabilitation Tool components

The tool design enables physicians to teach patients movements and support them during exercises at various stages of rehabilitation.

The tool consists of three parts: the Handheld attachment for physician control, which is directly attached to the flange of the robotic arm; the Linear slide for arm positioning, which has a semi-circular shape to allow the patient to easily rotate the arm for optimal exercise needs; and the arm support (passive rotary element), which is added to enable compliant movement and prevent discomfort during rehabilitation. In order to integrate the tool into our robot, we need to analyze its impact on our solution.

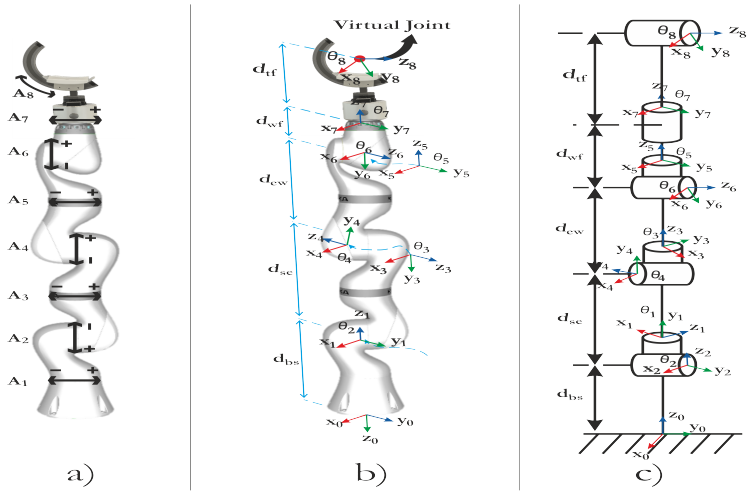

Fig. 1: Coordinate frames for Kuka LBR iiwa 7 R800: a) Joints Representation; b) Frames Representation; c) kinematic diagram

1.3 Integrating a Robotic Tool and Analyzing its Kinematics

Figure 1 depicts the kinematics of a robotic manipulator with n joints and n-1 links. A homogeneous transformation matrix represents each joint, specifying the necessary rotation or translation to align joint i-1 with joint i. We will concentrate on tool kinematics since the robot movement is well-defined. Figure 1 a) shows the addition of a tool with an extra virtual joint that poses stability challenges due to factors like strength and movement. These aspects will be reflected in the new Denavit-Hartenberg model for the solution.

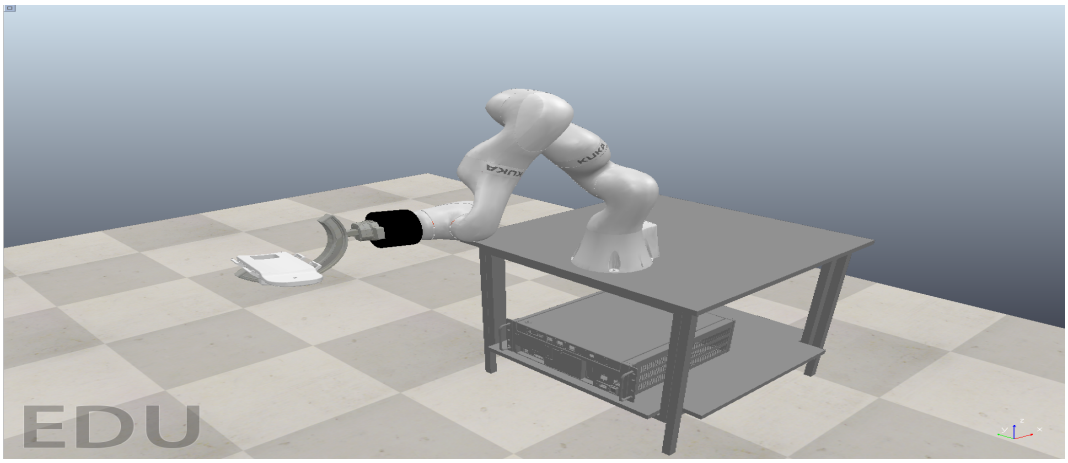

Fig. 2: Simulation Software setup of Robotic Arm with tool Integrated

Figure 2 depicts the simulation setup for the study, for the operation of this simulation approach a python connection was made to establish a control for the robotic arm and the aggregate tool which provide us with the necessary information to develop the respective Denavit-Hartenberg Model.

2 The Denavit-Hartenberg Model

The LBR iiwa 7 R800 from KUKA AG is one of the multiple robotic manipulators with 7-DoF that exists in the market, this robotic arm is characterized by using only rotary joints, i.e., it is a 7R redundant manipulator.

For the elaboration of the Denavit-Hartenberg parameters, the recreation of the assembly was recreated within the software V-Rep. With the addition and proper configuration of the eight joints of the robotic arm, we were able to obtain the following values:

Table 1: Denavit-Hartenberg Parameters

Link	a_i (rad)	α_i (mm)	d_i (mm)	θ_i (rad)
1	0	0	0	0
2	0	$\frac{\pi}{2}$	187.5	$-\pi$
3	0	$\frac{\pi}{2}$	0	π
4	0	$\frac{\pi}{2}$	400	0
5	0	$\frac{\pi}{2}$	0	$-\pi$
6	43.5	$-\frac{\pi}{2}$	400	$-\frac{\pi}{2}$
7	43.5	$-\pi$	0	$-\pi$
8	17.8	$-\pi$	395	$\frac{413\pi}{900}$

Table 1 shows the parameters obtained by the V-rep simulator for our solution.

3 Conclusions and Future Work

This article developed a Denavit-Hartenberg characteristic table 1 for a tool used in upper limb rehabilitation. The tool was introduced into a 3D simulation software where a further investigation will analyze the strength and effect that a patient will have on the robotic arm. This simulation study allows a better understanding of how to take advantage of the solution for patient rehabilitation and the addition of a virtual joint presents challenges to the stability of the robotic arm during movements. The developed characteristic table can help optimize the tool's performance, improving the understanding of exercise configuration for other studies [4] outcomes.

Acknowledgements

This work was funded by the projects "NORTE-01-0145- FEDER-000045" and "NORTE-01-0145-FEDER-000059", supported by Northern Portugal Regional Operational Programme (Norte2020), under the Portugal 2020 Partnership Agreement, through the

European Regional Development Fund (FEDER). It was also funded by national funds, through the FCT – Fundação para a Ciência e Tecnologia and FCT/MCTES in the scope of the project UIDB/05549/2020. The authors also acknowledge Fundação para a Ciência e a Tecnologia (FCT), Portugal and the European Social Found, European Union, for funding support through the "Programa Operacional Capital Humano" (POCH) in the scope of the PhD grant SFRH/BD/136721/2018 (B. Oliveira).

References

1. Nahid Norouzi-Gheidari, Philippe S. Archambault, and Joyce Fung. Effects of robot-assisted therapy on stroke rehabilitation in upper limbs: systematic review and meta-analysis of the literature. *Journal of rehabilitation research and development*, 49(4):479–496, jun 2012.
2. Irene Aprile, Arianna Cruciani, Marco Germanotta, Valerio Gower, Cristiano Pecchioli, Davide Cattaneo, Federica Vannetti, Luca Padua, and Furio Gramatica. Upper Limb Robotics in Rehabilitation: An Approach to Select the Devices, Based on Rehabilitation Aims, and Their Evaluation in a Feasibility Study. *Applied Sciences 2019, Vol. 9, Page 3920*, 9(18):3920, sep 2019.
3. Carlos Faria, Flora Ferreira, Wolfram Erlhagen, Sérgio Monteiro, and Estela Bicho. Position-based kinematics for 7-DoF serial manipulators with global configuration control, joint limit and singularity avoidance. *Mechanism and Machine Theory*, 121:317–334, mar 2018.
4. Marco Franceschini, Stefano Mazzoleni, Michela Goffredo, Sanaz Pournajaf, Daniele Galafate, Simone Criscuolo, Maurizio Agosti, and Federico Posteraro. Upper limb robot-assisted rehabilitation versus physical therapy on subacute stroke patients: A follow-up study. *Journal of Bodywork and Movement Therapies*, 24(1):194–198, jan 2020.

Development of a breast ultrasound phantom for medical training

Andreia Caldas, Simão Valente[1], Nuno S. Rodrigues[1], Augusto R. V. F. de Araújo[1], Rolands Strozs[1], Pedro Morais[1], Demétrio Matos[1], and João L. Vilaça[1]

Instituto Politécnico do Cávado e do Ave, IPCA, Portugal
amcaldas@ipca.pt

Abstract. Ultrasound (US) phantoms are models that aim to simulate human tissues with the same or similar acoustic properties. They are used for training clinical procedures, diagnostic techniques and testing and calibration of new systems. Some models for these purposes can be found in the literature, but their reproducibility in terms of lesion placement is restricted. This work aims to construct a breast phantom to plan and train breast biopsy. The presented study focuses on the design and production of the breast phantom with lesion for healthcare practices. This phantom will be used for training with new US systems and devices for needle insertion during breast biopsy. This technique focuses on the correct representation of a base model and positioning reproducibility of the lesion. This work contributes with a strategy for the development of a breast phantom constructed by pour-in-mold approach using US-compatible materials and the validation of the method to produce a low-cost and easy to produce breast phantom.

Keywords: phantom · breast phantom · ultrasound-compatible phantom · medical training · tissue-mimicking materials

1 Breast Phantom

1.1 Methods and Experiments

We propose a strategy to construct a synthetic breast phantom compatible with US using a pour-in-mold approach (Figure 1) [1, 2].

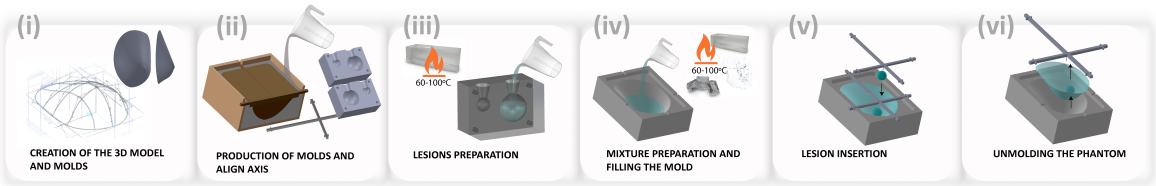

Fig. 1: Phantom construction.

Based on the literature, an ideal 3D breast model was created in SolidWorks [3, 4]. This model is used as a reference for molds creation and after 3D printed. Madsen et al. [5] to align the lesion, in the mold used to fill with the mixture that mimic the tissues, four depressions on each side of the mold were created to enable the fitting of an axis that supports the lesion with a thin stainless steel wire that is inserted in

the center of the axis in order to align the lesion.To simulate the tissues was used a mixture made with 30% Ballistic Gel and 70% Humimic Gel. The Ballistic Gel used was the Clear Ballistics 10% Synthetic Ballistic Gelatin and the Humimic Gel No. 4 given its similar acoustic characteristics with the breast tissues [6]. To make the US image more realistic and better distinguish the soft tissues of the lesion Glycerin (Lacrilar, Ramalhal, Portugal) was added [7]. Inspired by Morais et. Al. [8] two experiments were set to validate the proposed methodology. The first experiment evaluated the relative volume and positioning error of the breast and lesion. In the second experiment, the US images obtained from the phantom were qualitatively compared with the real breast US images.

1.2 Results

With these experiments were presenting the minimum and the maximum error relative to the breast and lesion volume, also giving the error relative to the method used for lesion positioning. The described methodology allows the construction of a phantom with an error of 1.47 +/- 0.78mm in the breast surface, compared to the ideal model (i.e. CAD version) (Figure 2). Concerning the lesion's centroid, an error of 0.52 +/- 0.23mm was detected. The qualitative evaluation (Figure 3) of the US images indicates that the phantom created do not exhibit an accurate heterogeneity of the real breast. Nonetheless, present comparable US images to those are commercially available from CIRS (Norfolk, VA, USA) [9]. In these phantoms, only the tumor can be distinguished from the surrounding tissues, while no differentiation between adipose and fibroglandular tissues is evident.

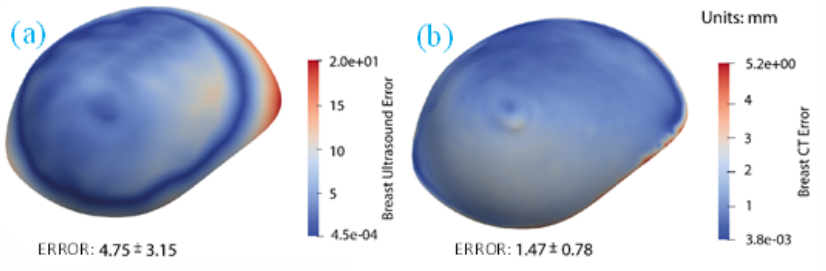

Fig. 2: Volume 3D color mapping- overlap (a) 3DUS, and (b) CT

1.3 Conclusions and Future Work

The described strategy proved to be an accurate and fast production of a low-cost model to be used in the training of breast biopsy procedures. Several topics are set to be explored in future experiments. These include improving the accuracy of breast models by incorporating real breast ultrasound volumes; obtaining a more in-depth understanding of the proposed mixture's behavior during needle insertion, regeneration properties and degradation over time.

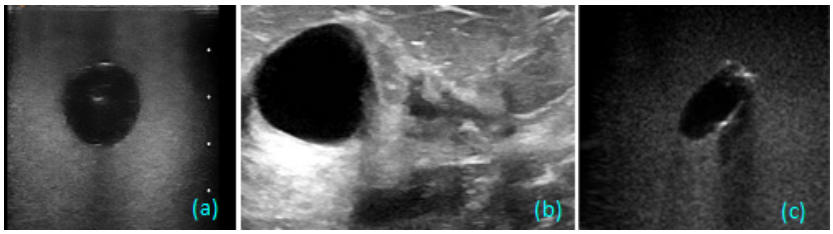

Fig. 3: US images (a) Phantom (b) Real breast [10] (c) CIRS phantom [9]

Acknowledgements

This project was funded by the projects "NORTE-01-0145-FEDER-000045" and "NORTE-01-0145-FEDER-000059", supported by Northern Portugal Regional Operational Programme (Norte2020), under the Portugal 2020 Partnership Agreement, through the European Regional Development Fund (ERDF). It was also financed by national funds, through FCT - Foundation for Science and Technology and FCT / MCTES under the project UIDB / 05549/2020, UIDP/05549/2020, CEECINST/00039/2021 and LASI-LA/P/0104/2020. This project was also funded by the Innovation Pact HfFP – Health From Portugal, co-funded from the "Mobilizing Agendas for Business Innovation" of the "Next Generation EU" program of Component 5 of the Recovery and Resilience Plan (RRP), concerning "Capitalization and Business Innovation", under the Regulation of the Incentive System "Agendas for Business Innovation".

References

1. Martin O. Culjat, David Goldenberg, Priyamvada Tewari, and Rahul S. Singh. A review of tissue substitutes for ultrasound imaging. *Ultrasound in Medicine and Biology*, 36(6):861–873, 2010.
2. Louise M. Cannon, Andrew J. Fagan, and Jacinta E. Browne. Novel tissue mimicking materials for high frequency breast ultrasound phantoms. *Ultrasound in Medicine and Biology*, 37(1):122–135, 2011.
3. British Standarts Institution. BS EN 13402-3 : Size designation of clothes, 2017.
4. Anita Ringberg, Erika Bågeman, Carsten Rose, Christian Ingvar, and Helena Jernström. Of cup and bra size: Reply to a prospective study of breast size and premenopausal breast cancer incidence. *International Journal of Cancer*, 119(9):2242–2243, 2006.
5. Ernest L. Madsen, Wendie A. Berg, Ellen B. Mendelson, and Gary R. Frank. Anthropomorphic breast phantoms for qualification of investigators for ACRIN protocol 6666. *Radiology*, 239(3):869–874, 2006.
6. Humimic Medical. Medical Gels.
7. Luciana C. Cabrelli, Felipe W. Grillo, Diego R.T. Sampaio, Antonio A.O. Carneiro, and Theo Z. Pavan. Acoustic and Elastic Properties of Glycerol in Oil-Based Gel Phantoms. *Ultrasound in Medicine and Biology*, 43(9):2086–2094, 2017.
8. P. Morais, J. M. R. S. Tavares, S. Queirós, F. Veloso, J. D'hooge, and J. L. Vilaça. Development of a patient-specific atrial phantom model for planning and training of inter-atrial interventions. *Medical Physics*, 44(11):5638–5649, 2017.
9. Sun Nuclear- A Mirion Medical Company. Ultrasound needle breast biopsy phantom with amorphous lesions, 2023.
10. Dataset of breast ultrasound images. *Data in Brief*, 28, feb 2020.

Deep Learning Methods for Lesion Detection on Full Screening Mammography: A Comparative Analysis

Raul Ferrete Ribeiro[1,2], Helena R. Torres[1,2,3,4], Bruno Oliveira[1,2,3,4], Pedro Morais[1,2], and João L. Vilaça[1,2]

[1] 2Ai – School of Technology, IPCA, Barcelos, Portugal
rmribeiro@ipca.pt, htorres@ipca.pt, boliveira@ipca.pt, pmorais@ipca.pt, jvilaca@ipca.pt
[2] LASI – Associate Laboratory of Intelligent Systems, Guimarães, Portugal
[3] Algoritmi Center, School of Engineering, University of Minho, Guimarães, Portugal
[4] ICVS - Life and Health Sciences Research Institute, School of Medicine, University of Minho, Braga, Portugal

Abstract. Breast cancer is the most prevalent type of cancer in women. Although mammography is used as the main imaging modality for the diagnosis, robust lesion detection in mammography images is a challenging task, due to the poor contrast of the lesion boundaries and the widely diverse sizes and shapes of the lesions. Deep Learning techniques have been explored to facilitate automatic diagnosis and have produced outstanding outcomes when used for different medical challenges. This study provides a benchmark for breast lesion detection in mammography images. Five state-of-art methods were evaluated on 1592 mammograms from a publicly available dataset (CBIS-DDSM) and compared considering the following seven metrics: i) mean Average Precision (mAP); ii) intersection over union; iii) precision; iv) recall; v) True Positive Rate (TPR); and vi) false positive per image. The CenterNet, YOLOv5, Faster-R-CNN, EfficientDet, and RetinaNet architectures were trained with a combination of the L1 localization loss and L2 localization loss. Despite all evaluated networks having mAP ratings greater than 60%, two managed to stand out among the evaluated networks. In general, the results demonstrate the efficiency of the model CenterNet with Hourglass-104 as its backbone and the model YOLOv5, achieving mAP scores of 70.71% and 69.36%, and TPR scores of 96.10% and 92.19%, respectively, outperforming the state-of-the-art models.

Keywords: Breast Cancer · Mammography · Object Detection · Deep Learning.

1 Object Detection in Mammography

The robust lesion detection of mammography images has been considered a backbreaking task due to: i) poor contrast of the lesion boundaries; ii) the extremely variable lesions' sizes and shapes; and iii) some extremely small lesions on the mammogram image [1]. To overcome these drawbacks, Deep Learning (DL) methods have been implemented and have shown impressive results when applied to medical image [2]. This work presents a benchmark for breast lesion detection in mammography images, where five state-of-the-art methods were evaluated on 1692 mammograms from a public dataset Curated Breast Imaging Subset Digital Database for Screening Mammography (CBIS-DDSM), and compared considering the following seven metrics: i) Intersection over Union (IoU); ii) Precision (Pre); iii) Recall (Rec); iv) mean Average Precision (mAP); v) True Positive Rate (TPR); vi) False Positive per Image (FPPI); and vii) Inference Time (IT). The Faster R-CNN [3], You Only Look Once (YOLO) [4], EfficientDet [5], CenterNet [6], and RetinaNet [7], architectures were trained with a combination of the L1 localization loss and L2 localization loss for the bounding box. In general, the results

(Figure 1, Table 1) demonstrate the efficiency of the model CenterNet with Hourglass-104 as its backbone and the model YOLOv5, achieving mAP scores of 70.71% and 69.36%, and TPR scores of 96.10% and 92.19%, respectively, outperforming the state-of-the-art models

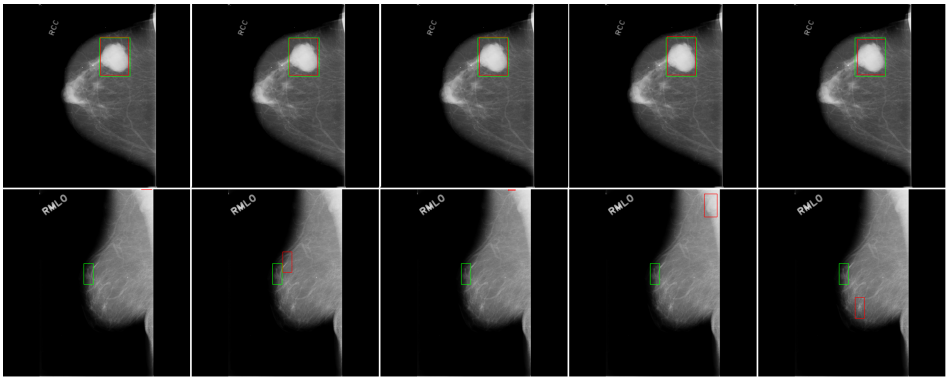

Fig. 1: Results of the networks evaluated on the lesion detection task. An example of good, and bad detection results are presented (green: ground truth, red: prediction).

Table 1: Comparison of the Different DL Methods

Networks	**Backbones**	**Input size**	**Evaluation Metrics**			
			mAP	**TPR**	**FPPI**	**IT (ms)**
CenterNet	**HourGlass104**	640	64.22	93.39	0.54	9.37
		1024	**70.71**	**96.10**	0.49	10.39
YOLOV5	**CSP-Darknet53**	640	69.36	92.19	0.48	**2.11**
		1024	68.60	86.79	**0.44**	3.12
Faster R-CNN	**Resnet50**	640	60.49	83.78	0.62	6.76
		1024	62.40	86.49	0.57	10.83
	Resnet152	640	64.54	83.18	0.48	8.10
		1024	66.02	89.49	0.53	14.71
EfficientDet	**D1**	640	64.81	93.09	0.61	6.56
		1024	68.78	90.69	0.49	7.57
RetinaNet	**Resnet50**	640	54.26	77.77	0.70	5.71
		1024	50.30	95.20	1.05	6.28

Acknowledgements

This project was funded by the projects “NORTE-01-0145-FEDER-000045” and “NORTE-01-0145-FEDER-000059”, supported by Northern Portugal Regional Operational Programme (Norte2020), under the Portugal 2020 Partnership Agreement, through the

European Regional Development Fund (ERDF). It was also financed by national funds, through FCT - Foundation for Science and Technology and FCT / MCTES under the project UIDB / 05549/2020, UIDP/05549/2020, CEECINST/00039/2021 and LASI-LA/P/0104/2020. This project was also funded by the Innovation Pact HfFP – Health From Portugal, co-funded from the "Mobilizing Agendas for Business Innovation" of the "Next Generation EU" program of Component 5 of the Recovery and Resilience Plan (RRP), concerning "Capitalization and Business Innovation", under the Regulation of the Incentive System "Agendas for Business Innovation". The authors also acknowledge FCT, Portugal and the European Social Fund, European Union, for funding support through the "Programa Operacional Capital Humano" (POCH) in the scope of the PhD grants SFRH/BD/136721/2018 (B. Oliveira) and SFRH/BD/136670 (H.R. Torres).

References

1. Neeraj Dhungel, Gustavo Carneiro, and Andrew P. Bradley. A deep learning approach for the analysis of masses in mammograms with minimal user intervention. *Medical Image Analysis*, 37:114–128, 2017.
2. Andres Anaya-Isaza, Leonel Mera-Jimenez, Johan Manuel Cabrera-Chavarro, Lorena Guachi-Guachi, Diego Peluffo-Ordonez, and Jorge Ivan Rios-Patino. Comparison of current deep convolutional neural networks for the segmentation of breast masses in mammograms. *IEEE Access*, 9:152206–152225, 2021.
3. Shaoqing Ren, Kaiming He, Ross Girshick, and Jian Sun. Faster r-cnn: Towards real-time object detection with region proposal networks. *IEEE Transactions on Pattern Analysis and Machine Intelligence*, 39:1137–1149, 2015.
4. Joseph Redmon, Santosh Divvala, Ross Girshick, and Ali Farhadi. You only look once: Unified, real-time object detection. *Proceedings of the IEEE Computer Society Conference on Computer Vision and Pattern Recognition*, 2016-December:779–788, 2015.
5. Mingxing Tan, Ruoming Pang, and Quoc V. Le. Efficientdet: Scalable and efficient object detection. 2019.
6. Kaiwen Duan, Song Bai, Lingxi Xie, Honggang Qi, Qingming Huang, and Qi Tian. Centernet: Keypoint triplets for object detection. *Proceedings of the IEEE International Conference on Computer Vision*, 2019-October:6568–6577, 2019.
7. Tsung Yi Lin, Priya Goyal, Ross Girshick, Kaiming He, and Piotr Dollar. Focal loss for dense object detection. *IEEE Transactions on Pattern Analysis and Machine Intelligence*, 42:318–327, 2017.

Comparative Analysis of Deep Learning Networks for Lesion Classification in Breast Ultrasound Images

Margarida Ferreira[1,2], Helena Torres[1,2,3,4], Bruno Oliveira[1,2,3,4], Augusto Araújo[1], Pedro Morais[1,3], Paulo Novais[2,3], and João Vilaça[1,3]

[1] 2Ai, Instituto Politécnico do Cávado e do Ave, Portugal
{amrferreira, htorres, boliveira, avferreira, pmorais, jvilaca}@ipca.pt
[2] Algoritmi Center, School of Engineering, University of Minho, Portugal
pjon@di.uminho.pt
[3] LASI – Associate Laboratory of Intelligent Systems, Portugal
[4] ICVS - Life and Health Sciences Research Institute, University of Minho, Portugal

Abstract. Accurate breast lesion classification in ultrasound (US) images is a critical task for breast cancer diagnosis but requires experienced medical professionals and has many challenges, such as poor image quality, artifacts, and high lesion variability. Thus, automatic lesion classification through computer-aided diagnosis systems may aid in medical image interpretation and, consequently, in breast cancer diagnosis. Recently, such systems using convolutional neural networks (CNNs) have demonstrated remarkable results in breast lesion classification tasks, outperforming the intra and inter-observer variability. Although several methods have been proposed, most studies used small private datasets with different quantitative metrics, limiting the comparison between approaches. This work is a benchmark for breast lesion classification in US images comparing six state-of-the-art CNNs. For each network, five input data variations were implemented and compared. The methods were trained on a multi-center breast US dataset and evaluated using five metrics. Overall, the input data representing the lesion with a thin border of background provides the best performance using EfficientNet, obtaining an accuracy of 97.65% and an area under the curve of 96.30%.

Keywords: Breast cancer · Classification · Deep learning · Ultrasound.

1 Lesion Classification in Ultrasound

In order to fill a gap in the existing literature, this work presents a benchmark for lesion classification in breast US images comparing six state-of-the-art networks: GoogLeNet [1], InceptionV3 [2], ResNet [3], DenseNet [4], MobileNetV2 [5], and EfficientNet [6]. Figure 1 shows a graphical summary of the comparative study.

For each network, five input data variations (Inputs A, B, C, D, and E represented in Figure 1) that include segmentation information were assessed to compare their impact on the final performance. The methods were trained on a multi-center breast US dataset, composed of BUSI and UDIAT datasets, containing 547 benign lesions and 263 malignant lesions, and evaluated using the following metrics: precision, sensitivity, F1-score, accuracy, and area under the curve (AUC). Each network was trained for 5000 epochs with a batch size of 10, using the cross-entropy loss function and Adam optimizer with a learning rate of 1e-4. In addition, to prevent overfitting and improve performance, the train set was subjected to data augmentation.

2 Results and Discussion

Table 1 presents the results for the five image variations used as input to each network.

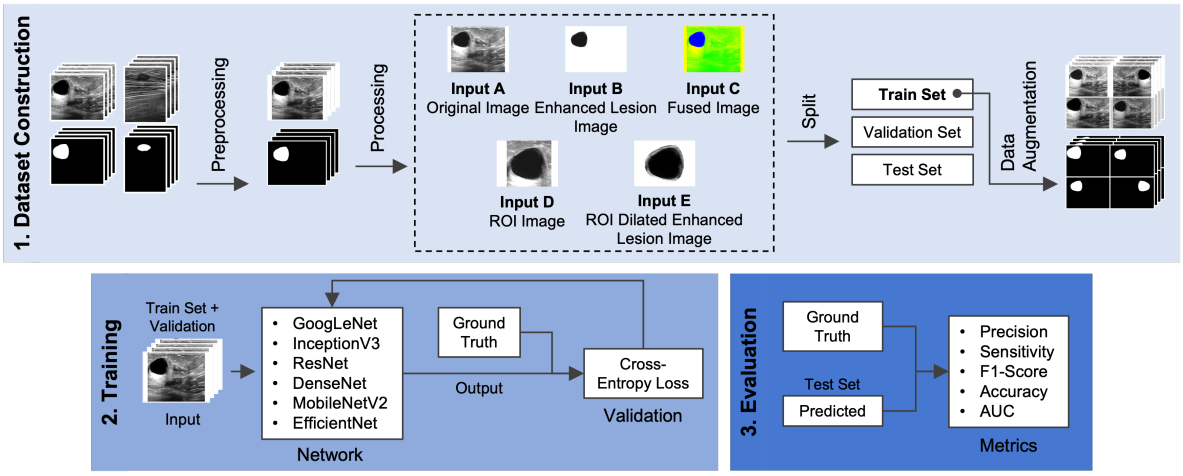

Fig. 1: Graphical summary of the classification comparative study.

EfficientNet delivered the best performance for most input data variations, as it is a recent and highly efficient architecture that achieves state-of-the-art performance at low processing load and training speed. EfficientNet trained using Input E, the lesion with a thin border of background, achieved the best overall performance, obtaining a precision, sensitivity, F1-score, accuracy, and AUC of 97.73%, 97.65%, 97.62%, 97.65%, and 96.30%, respectively. Since the US background adds entropy to the image, its exclusion benefits the classification task, and the border gives clues to identify the lesion's nature. The results corroborate the added value of deep learning strategies, particularly EfficientNet, for breast US lesion classification and, ultimately, for breast cancer diagnosis.

Acknowledgements

This project was funded by the projects "NORTE-01-0145-FEDER-000045" and "NORTE-01-0145-FEDER-000059", supported by Northern Portugal Regional Operational Programme (Norte2020), under the Portugal 2020 Partnership Agreement, through the European Regional Development Fund (ERDF). It was also financed by national funds, through FCT - Foundation for Science and Technology and FCT / MCTES under the project UIDB/05549/2020, UIDP/05549/2020, CEECINST/00039/2021 and LASI-LA/P/0104/2020. This project was also funded by the Innovation Pact HfFP – Health From Portugal, co-funded from the "Mobilizing Agendas for Business Innovation" of the "Next Generation EU" program of Component 5 of the Recovery and Resilience Plan (RRP), concerning "Capitalization and Business Innovation", under the Regulation of the Incentive System "Agendas for Business Innovation". The authors also acknowledge FCT, Portugal and the European Social Fund, European Union, for funding support through the "Programa Operacional Capital Humano" (POCH) in the scope of the PhD grants SFRH/BD/136721/2018 (B. Oliveira) and SFRH/BD/136670 (H. R. Torres). A. R. V. F. de Araújo thanks CAPES Brazilian Foundation for supporting his graduation course.

Table 1: Quantitative comparison of the networks using the input data variations.

Input Data Variations	Networks	Evaluation Metrics				
		Precision	Sensitivity	F1-Score	Accuracy	AUC
Input A	GoogLeNet	86.58	86.42	86.49	86.42	84.93
	InceptionV3	90.03	90.12	90.01	90.12	87.66
	ResNet	78.38	79.01	78.35	79.01	73.39
	DenseNet	89.46	91.61	90.37	91.36	91.61
	MobileNetV2	86.11	85.19	85.43	85.19	85.03
	EfficientNet	**93.32**	**92.59**	**92.72**	**92.59**	**93.53**
Input B	GoogLeNet	96.29	96.29	96.28	96.30	95.24
	InceptionV3	95.06	95.06	95.06	95.06	94.34
	ResNet	95.72	95.06	95.14	95.06	96.36
	DenseNet	96.29	96.29	96.28	96.30	95.24
	MobileNetV2	95.06	95.06	95.06	95.06	94.34
	EfficientNet	**97.62**	**97.53**	**97.50**	**97.53**	**96.15**
Input C	GoogLeNet	87.65	87.65	87.65	87.65	85.84
	InceptionV3	87.65	87.65	87.65	87.65	85.84
	ResNet	82.04	80.25	80.70	80.25	80.38
	DenseNet	90.12	90.12	90.12	90.12	88.67
	MobileNetV2	92.59	92.59	92.59	92.59	91.50
	EfficientNet	**95.28**	**95.06**	**95.11**	**95.06**	**95.35**
Input D	GoogLeNet	**92.94**	**92.94**	**92.94**	**92.94**	**91.86**
	InceptionV3	89.93	89.41	89.55	89.41	89.27
	ResNet	80.87	81.18	80.97	81.18	77.30
	DenseNet	89.33	89.41	89.36	89.41	87.29
	MobileNetV2	89.32	89.41	89.23	89.41	86.30
	EfficientNet	91.76	91.76	91.63	91.76	89.02
Input E	GoogLeNet	95.32	95.29	95.24	95.29	93.58
	InceptionV3	96.47	96.47	96.45	96.47	95.43
	ResNet	94.09	94.12	94.09	94.12	92.72
	DenseNet	94.20	94.12	94.15	94.12	93.71
	MobileNetV2	94.20	94.12	94.02	94.12	91.73
	EfficientNet	**98.84**	**98.82**	**98.82**	**98.82**	**98.15**

References

1. Christian Szegedy, Wei Liu, Yangqing Jia, Pierre Sermanet, Scott Reed, Dragomir Anguelov, Dumitru Erhan, Vincent Vanhoucke, and Andrew Rabinovich. Going deeper with convolutions. In *2015 IEEE Conference on Computer Vision and Pattern Recognition (CVPR)*, pages 1–9. IEEE, jun 2015.
2. Christian Szegedy, Vincent Vanhoucke, Sergey Ioffe, Jon Shlens, and Zbigniew Wojna. Rethinking the Inception Architecture for Computer Vision. In *Proceedings of the IEEE Computer Society Conference on Computer Vision and Pattern Recognition*, pages 2818–2826. IEEE Computer Society, dec 2016.
3. Kaiming He, Xiangyu Zhang, Shaoqing Ren, and Jian Sun. Deep residual learning for image recognition. In *Proceedings of the IEEE Computer Society Conference on Computer Vision and Pattern Recognition*, pages 770–778. IEEE Computer Society, dec 2016.
4. Gao Huang, Zhuang Liu, Laurens Van Der Maaten, and Kilian Q. Weinberger. Densely Connected Convolutional Networks. In *2017 IEEE Conference on Computer Vision and Pattern Recognition (CVPR)*, pages 2261–2269. IEEE, jul 2017.
5. Mark Sandler, Andrew Howard, Menglong Zhu, Andrey Zhmoginov, and Liang Chieh Chen. MobileNetV2: Inverted Residuals and Linear Bottlenecks. *Proceedings of the IEEE Computer Society Conference on Computer Vision and Pattern Recognition*, pages 4510–4520, 2018.
6. Mingxing Tan and Quoc V. Le. EfficientNet: Rethinking model scaling for convolutional neural networks. *36th International Conference on Machine Learning, ICML 2019*, pages 10691–10700, 2019.

Remote monitoring system of dynamic compression bracing to correct pectus carinatum

António Real[1,2], Pedro Morais[1,2], Bruno Oliveira[1,2,3,4], Helena R. Torres[1,2,3,4], and João L. Vilaça[1,2]

[1] 2Ai – School of Technology, IPCA, Barcelos, Portugal
areal@ipca.pt, pmorais@ipca.pt, boliveira@ipca.pt, htorres@ipca.pt, jvilaca@ipca.pt
[2] LASI – Associate Laboratory of Intelligent Systems, Guimarães, Portugal
[3] Algoritmi Center, School of Engineering, University of Minho, Guimarães, Portugal
[4] ICVS - Life and Health Sciences Research Institute, School of Medicine, University of Minho, Braga,Portugal

Abstract. Pectus carinatum (PC) is a chest deformity caused by disproportionate growth of the costal cartilages compared with the bony thoracic skeleton, pulling the sternum forwards and leading to its protrusion. Currently, the most common non-invasive treatment is external compressive bracing, by means of an orthosis. While this treatment is widely adopted, the correct magnitude of applied compressive forces remains unknown, leading to suboptimal results. Moreover, the current orthoses are not suitable to monitor the treatment. The purpose of this study is to design a force measuring system that could be directly embedded into an existing PC orthosis without relevant modifications in its construction. For that, inspired by the currently commercially available products where a solid silicone pad is used, three concepts for silicone-based sensors, two capacitive and one magnetic type, are presented and compared. Additionally, a concept of a full pipeline to capture and store the sensor data was researched. Compression tests were conducted on a calibration machine, with forces ranging from 0 N to 300 N. Overall, the proposed system demonstrated its potential to measure and monitor orthosis' applied forces, corroborating its potential for clinical practice.

Keywords: Pectus Carinatum · Capacitive Sensing · Magnetometer · Pressure · Continuous Monitoring.

1 Monitoring of compressive forces of bracing system

The incidence rate of pectus carinatum is 1:1000 births [1] and is more common in males than females with a ratio of about 4:1 [2]. The primary non-invasive treatment option for this deformity is the use of compressive bracing applied by orthoses which consist of one or more aluminium/steel bar, a cushioned pad, back and shoulder straps. This type of orthoses has demonstrated its good results in recent years [3] [4] however it has been reported that a large number of patients do not follow the clinically prescribed treatment (e.g. applied pressure, usage time) [5]. Moreover, the systems are blind, not monitoring the applied pressure. While too much pressure can cause pain and pressure ulcers in the patient, inadequate pressure will prolong treatment time and will result in a sub-optimal outcome and consequently some loss of confidence in the treatment outcome. To overcome these drawbacks, this work presents sensors embedded in the cushioning pad that can be used for monitoring the forces applied to the chest. Three sensors concepts were tested, two based on capacitive technology and one based on magnetometers (Figure 1). To evaluate the response of the sensors when force is applied, they were subjected to compressive forces ranging from 0N to 300N using a 10kN load

cell (AGS-X, Shimadzu, Kyoto, Japan) and the results (Figure 2) show all the sensors have high linearity. The foam-based showed the highest sensibility and to correctly test the feasibility of the proposed devices, a clinical study is expected to be conducted in PC patients during the next months.

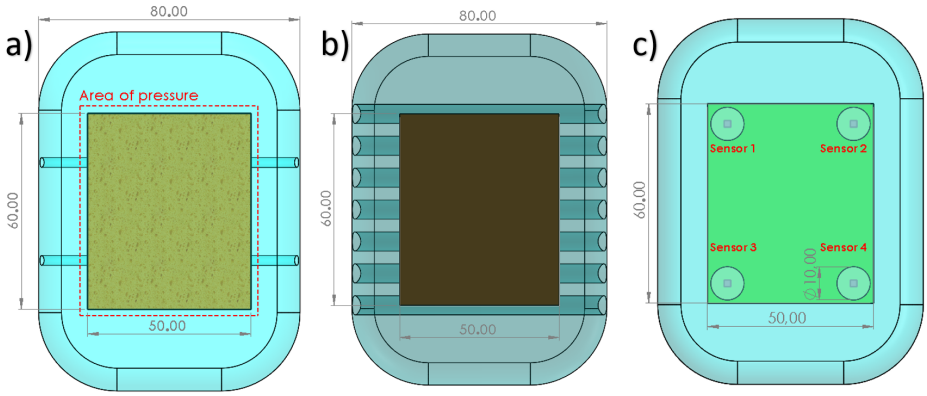

Fig. 1: Experimental force sensors embedded in silicon pad, a) Capacitive foam-based sensor, b) Perforated silicon capacitive sensor, c) Magnetometer-based sensor.

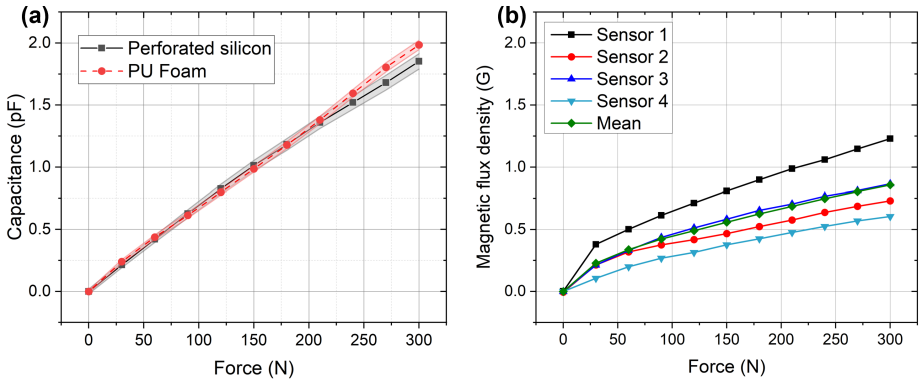

Fig. 2: a) Changing capacitance as a function of compressive force for both capacitive sensors, filled area represents standard deviation, b) Magnetic flux density measured on the Z axis as a function of force on magnetometers

Acknowledgements

This project was funded by the projects "NORTE-01-0145-FEDER-000045" and "NORTE-01-0145-FEDER-000059", supported by Northern Portugal Regional Operational Programme (Norte2020), under the Portugal 2020 Partnership Agreement, through the European Regional Development Fund (ERDF). It was also financed by national funds,

through FCT - Foundation for Science and Technology and FCT / MCTES under the project UIDB / 05549/2020, UIDP/05549/2020, CEECINST/00039/2021 and LASI-LA/P/0104/2020. This project was also funded by the Innovation Pact HfFP – Health From Portugal, co-funded from the "Mobilizing Agendas for Business Innovation" of the "Next Generation EU" program of Component 5 of the Recovery and Resilience Plan (RRP), concerning "Capitalization and Business Innovation", under the Regulation of the Incentive System "Agendas for Business Innovation". The authors also acknowledge FCT, Portugal and the European Social Fund, European Union, for funding support through the "Programa Operacional Capital Humano" (POCH) in the scope of the PhD grants SFRH/BD/136721/2018 (B. Oliveira) and SFRH/BD/136670 (H.R. Torres).

References

1. Emanuele Russo, Alessandro Bertani, Lavinia De Monte, and Francesco Raffaele. Pectus carinatum. *Plastic and Cosmetic Surgery of the Male Breast*, 2020.
2. Thomas J. Desmarais and Martin S. Keller. Pectus carinatum, 2013.
3. Sara Colozza and Andreana Bütter. Bracing in pediatric patients with pectus carinatum is effective and improves quality of life. 2013.
4. Richy T. Lee, Scott Moorman, Marc Schneider, and David L. Sigalet. Bracing is an effective therapy for pectus carinatum: Interim results. *Journal of Pediatric Surgery*, 2013.
5. Bracing of pectus carinatum: A quantitative analysis. *Journal of Pediatric Surgery*, 2018.

AI for Detection of Illegal Soccer Streams

Diogo Pontes[1], Claudino Costa[1], Miguel Santos Marques[1], Helena A. Correia[1], João Rodrigues[1], and José Henrique Brito[1,2]

[1] 2Ai – School of Technology, IPCA, Barcelos, Portugal
dpontes@ipca.pt , cbcosta@ipca.pt , msmarques@ipca.pt , hacorreia@ipca.pt , jtrodrigues@ipca.pt , jbrito@ipca.pt
[2] LASI – Associate Laboratory of Intelligent Systems, Guimarães, Portugal

Abstract. This study presents the earlier steps in the detection of pirate soccer streams using computer vision. The focus of this study is the Portuguese market, therefore the majority of work relates to the country's major soccer competitions and TV broadcasters. The study employs 5 tasks: Shot Classification, Object Detection, Player Tracking, Field Segmentation and Player Parsing. Shot Classification represent a task that aims to classify the type of view broadcasted on a soccer video and uses a neural network. Object Detection aims to detect typical evidences on a soccer stream, as scoreboard, competition logo and TV channel using a object detector. The Player Tracking main goal is to track players on the field, re-identifying when they are occluded or leave the scenario. Field segmentation will work along side with Tracking, limiting field area segmenting lines, extremities and areas using U-Net. Finally, parsing have two main goals, player identification using player face similarity and team identification through jersey team color using MediaPipe for player segmentation and a histogram for color classification. The proposed results/experiments are presented with some examples.

Keywords: Soccer Video · Shot Classification · Object Detection · Player Tracking · Field Segmentation · Parsing

1 System Blocks

This study proposes stages of identifying illegal soccer streams using computer vision, through evidences provided by the game, for example scoreboard, players recognition, TV channel, among others, concentrating on the Portuguese market and aims mainly on the country's major soccer leagues and TV channels. The study employs 5 tasks: Shot Classification, Object Detection, Player Tracking, Field Segmentation and Player Parsing.

The first task, Shot Classification, is responsible for identifying the type of view broadcasted on a soccer video. The classifier is built upon DenseNet201 [2], trained on a expanded version of the dataset SoccerNet-V2 [1]. The dataset was modified into three classes: "close shot"(Fig. 1.a), "other"(Fig. 1.b) and "wide shot"(Fig. 1.c).

The second task, Object Detection, aims to identify visuals elements that help identify a soccer match, using Yolov5. In this study we focus on the identification of logos that are prominent for the entire 90 minutes of the match, those are: broadcaster logo, competition logo and scoreboards. In Fig. 1.d is given an example of scoreboard detection. A custom dataset was created using images extracted from online sources and publicly available content, such as YouTube and Twitter.

The third task, Player Tracking, is focused on tracking players on the field. The algorithm used is called ByteTrack [5], and it is responsible for re-identifying players when they are occluded or leave the scenario, illustrated on Fig. 1.d.

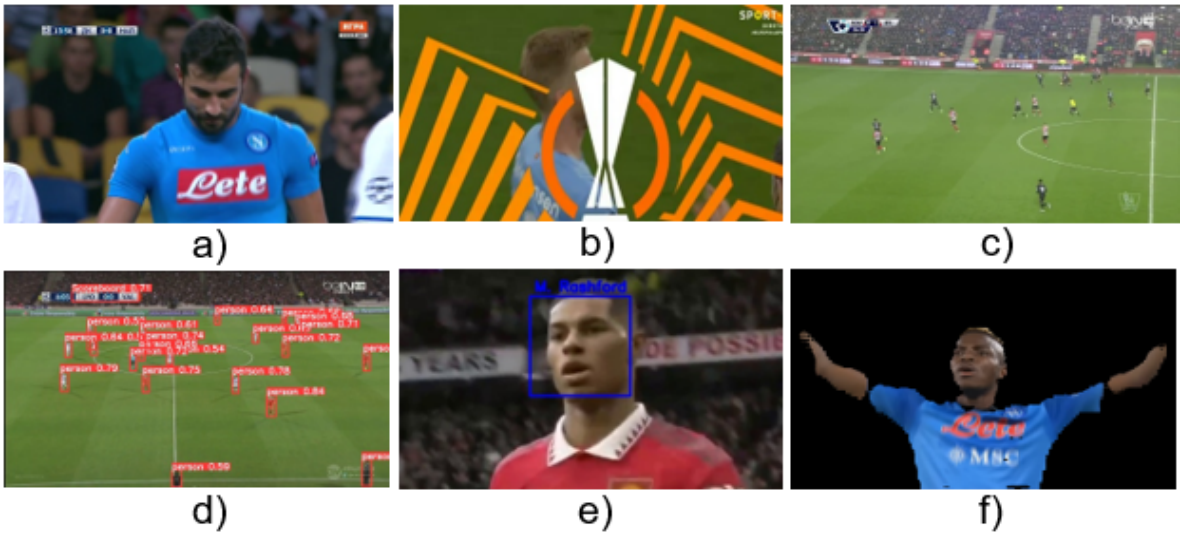

Fig. 1: Types of shot classification: (a) Close-up Shot, (b) Other and (c) Wide Shot. (d) Scoreboard Detection and Tracking. (e) Player Face Recognition. (f) Jersey segmentation for Team Parsing. Images from SoccerNetV2 [1] and our dataset.

The fourth task, Field Segmentation, works alongside Player Tracking, segmenting the field area and limiting it to specific lines, extremities, and areas using the U-Net algorithm [4], illustrated on Fig. 2.

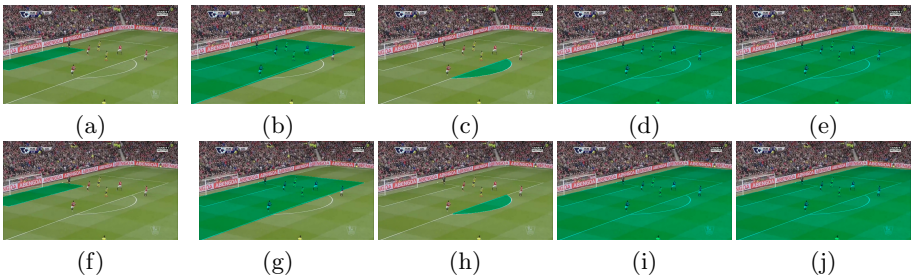

Fig. 2: Segmentation results for a typical input image from a common viewpoint: (a)-(d) Groundtruth masks for areas on the left side of the pitch; (e) Groundtruth mask for whole field; (f)-(i) Predicted masks for the areas on the left side of the pitch; (j) Predicted mask for whole field.

Finally, the fifth task, Player Parsing, has two objectives. The first is to identify players through their face similarity using a siamese network, illustrated on Fig. 1.e. The second is to identify team jersey colors through the comparison of the HSV histogram with the reference color of the team jerseys. The HSV histogram is computed after the player is segmented from the background using the body segmentation model implemented in MediaPipe [3], illustrated on Fig. 1.f.

The proposed results and experiments are presented with visual examples. By using these techniques, the study aims to aid in the detection and prevention of illegal pirate soccer streams, specifically in the Portuguese market.

Acknowledgements

This work was partially funded by the project "POCI-01-0247-FEDER-046964", supported by Operational Program for Competitiveness and Internationalization (COMPETE 2020), under the PORTUGAL 2020 Partnership Agreement, through the European Regional Development Fund (ERDF 1). This work was also partially funded by national funds (PIDDAC), through the FCT – Fundação para a Ciência e Tecnologia and FCT/MCTES under the scope of the projects UIDB/05549/2020 and UIDP/05549/2020. This work was also partially funded by national funds, through the FCT – Fundação para a Ciência e a Tecnologia and FCT/MCTES under the scope of the project LASI-LA/P/0104/2020.

References

1. Deliège, A., Cioppa, A., Giancola, S., Seikavandi, M.J., Dueholm, J.V., Nasrollahi, K., Ghanem, B., Moeslund, T.B., Droogenbroeck, M.V.: Soccernet-v2 : A dataset and benchmarks for holistic understanding of broadcast soccer videos. In: The IEEE Conference on Computer Vision and Pattern Recognition (CVPR) Workshops (June 2021)
2. Huang, G., Liu, Z., van der Maaten, L., Weinberger, K.Q.: Densely connected convolutional networks (2018)
3. Lugaresi, C., Tang, J., Nash, H., McClanahan, C., Uboweja, E., Hays, M., Zhang, F., Chang, C.L., Yong, M., Lee, J., Chang, W.T., Hua, W., Georg, M., Grundmann, M.: Mediapipe: A framework for perceiving and processing reality. In: Third Workshop on Computer Vision for AR/VR at IEEE Computer Vision and Pattern Recognition (CVPR) 2019 (2019)
4. Ronneberger, O., P.Fischer, Brox, T.: U-net: Convolutional networks for biomedical image segmentation. In: Medical Image Computing and Computer-Assisted Intervention (MICCAI). LNCS, vol. 9351, pp. 234–241. Springer (2015)
5. Zhang, Y., Sun, P., Jiang, Y., Yu, D., Weng, F., Yuan, Z., Luo, P., Liu, W., Wang, X.: Bytetrack: Multi-object tracking by associating every detection box (2022)

Deep Learning Methods for Lesion Detection on Full Screening Mammography: A Comparative Analysis

Raul Ferrete Ribeiro[1,2], Helena R. Torres[1,2,3,4], Bruno Oliveira[1,2,3,4], Pedro Morais[1,2], and João L. Vilaça[1,2]

[1] Instituto Politécnico do Cávado e do Ave, IPCA, Portugal
rmribeiro@ipca.pt, htorres@ipca.pt, boliveira@ipca.pt, pmorais@ipca.pt, jvilaca@ipca.pt
[2] LASI – Associate Laboratory of Intelligent Systems, Guimarães, Portugal
[3] Algoritmi Center, School of Engineering, University of Minho, Guimarães, Portugal
[4] ICVS - Life and Health Sciences Research Institute, School of Medicine, University of Minho, Braga, Portugal

Abstract. Breast cancer is the most prevalent type of cancer in women. Although mammography is used as the main imaging modality for the diagnosis, robust lesion detection in mammography images is a challenging task, due to the poor contrast of the lesion boundaries and the widely diverse sizes and shapes of the lesions. Deep Learning techniques have been explored to facilitate automatic diagnosis and have produced outstanding outcomes when used for different medical challenges. This study provides a benchmark for breast lesion detection in mammography images. Five state-of-art methods were evaluated on 1592 mammograms from a publicly available dataset (CBIS-DDSM) and compared considering the following seven metrics: i) mean Average Precision (mAP); ii) intersection over union; iii) precision; iv) recall; v) True Positive Rate (TPR); and vi) false positive per image. The CenterNet, YOLOv5, Faster-R-CNN, EfficientDet, and RetinaNet architectures were trained with a combination of the L1 localization loss and L2 localization loss. Despite all evaluated networks having mAP ratings greater than 60%, two managed to stand out among the evaluated networks. In general, the results demonstrate the efficiency of the model CenterNet with Hourglass-104 as its backbone and the model YOLOv5, achieving mAP scores of 70.71% and 69.36%, and TPR scores of 96.10% and 92.19%, respectively, outperforming the state-of-the-art models.

Keywords: Breast Cancer · Mammography · Object Detection · Deep Learning.

1 Object Detection in Mammography

The robust lesion detection of mammography images has been considered a backbreaking task due to: i) poor contrast of the lesion boundaries; ii) the extremely variable lesions' sizes and shapes; and iii) some extremely small lesions on the mammogram image [1]. To overcome these drawbacks, Deep Learning (DL) methods have been implemented and have shown impressive results when applied to medical image [2]. This work presents a benchmark for breast lesion detection in mammography images, where five state-of-the-art methods were evaluated on 1692 mammograms from a public dataset Curated Breast Imaging Subset Digital Database for Screening Mammography (CBIS-DDSM), and compared considering the following seven metrics: i) Intersection over Union (IoU); ii) Precision (Pre); iii) Recall (Rec); iv) mean Average Precision (mAP); v) True Positive Rate (TPR); vi) False Positive per Image (FPPI); and vii) Inference Time (IT). The Faster R-CNN [3], You Only Look Once (YOLO) [4], EfficientDet [5], CenterNet [6], and RetinaNet [7], architectures were trained with a combination of the L1 localization loss and L2 localization loss for the bounding box. In general, the results

(Figure 1, Table 1) demonstrate the efficiency of the model CenterNet with Hourglass-104 as its backbone and the model YOLOv5, achieving mAP scores of 70.71% and 69.36%, and TPR scores of 96.10% and 92.19%, respectively, outperforming the state-of-the-art models

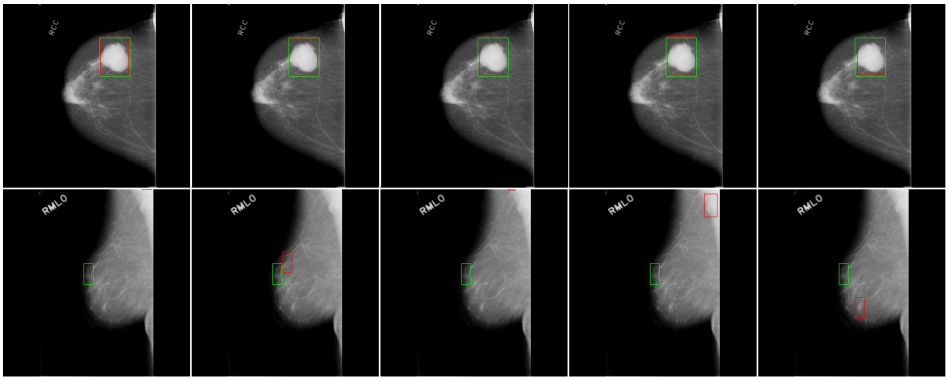

Fig. 1: Results of the networks evaluated on the lesion detection task. An example of good, and bad detection results are presented (green: ground truth, red: prediction).

Table 1: Comparison of the Different DL Methods

Networks	**Backbones**	**Input size**	**Evaluation Metrics**			
			mAP	**TPR**	**FPPI**	**IT (ms)**
CenterNet	**HourGlass104**	640	64.22	93.39	0.54	9.37
		1024	**70.71**	**96.10**	0.49	10.39
YOLOV5	**CSP-Darknet53**	640	69.36	92.19	0.48	**2.11**
		1024	68.60	86.79	**0.44**	3.12
Faster R-CNN	**Resnet50**	640	60.49	83.78	0.62	6.76
		1024	62.40	86.49	0.57	10.83
	Resnet152	640	64.54	83.18	0.48	8.10
		1024	66.02	89.49	0.53	14.71
EfficientDet	**D1**	640	64.81	93.09	0.61	6.56
		1024	68.78	90.69	0.49	7.57
RetinaNet	**Resnet50**	640	54.26	77.77	0.70	5.71
		1024	50.30	95.20	1.05	6.28

Acknowledgements

This project was funded by the projects “NORTE-01-0145-FEDER-000045” and “NORTE-01-0145-FEDER-000059”, supported by Northern Portugal Regional Operational Programme (Norte2020), under the Portugal 2020 Partnership Agreement, through the

European Regional Development Fund (ERDF). It was also financed by national funds, through FCT - Foundation for Science and Technology and FCT / MCTES under the project UIDB / 05549/2020, UIDP/05549/2020, CEECINST/00039/2021 and LASI-LA/P/0104/2020. This project was also funded by the Innovation Pact HfFP – Health From Portugal, co-funded from the "Mobilizing Agendas for Business Innovation" of the "Next Generation EU" program of Component 5 of the Recovery and Resilience Plan (RRP), concerning "Capitalization and Business Innovation", under the Regulation of the Incentive System "Agendas for Business Innovation". The authors also acknowledge FCT, Portugal and the European Social Fund, European Union, for funding support through the "Programa Operacional Capital Humano" (POCH) in the scope of the PhD grants SFRH/BD/136721/2018 (B. Oliveira) and SFRH/BD/136670 (H.R. Torres).

References

1. Neeraj Dhungel, Gustavo Carneiro, and Andrew P. Bradley. A deep learning approach for the analysis of masses in mammograms with minimal user intervention. *Medical Image Analysis*, 37:114–128, 2017.
2. Andres Anaya-Isaza, Leonel Mera-Jimenez, Johan Manuel Cabrera-Chavarro, Lorena Guachi-Guachi, Diego Peluffo-Ordonez, and Jorge Ivan Rios-Patino. Comparison of current deep convolutional neural networks for the segmentation of breast masses in mammograms. *IEEE Access*, 9:152206–152225, 2021.
3. Shaoqing Ren, Kaiming He, Ross Girshick, and Jian Sun. Faster r-cnn: Towards real-time object detection with region proposal networks. *IEEE Transactions on Pattern Analysis and Machine Intelligence*, 39:1137–1149, 2015.
4. Joseph Redmon, Santosh Divvala, Ross Girshick, and Ali Farhadi. You only look once: Unified, real-time object detection. *Proceedings of the IEEE Computer Society Conference on Computer Vision and Pattern Recognition*, 2016-December:779–788, 2015.
5. Mingxing Tan, Ruoming Pang, and Quoc V. Le. Efficientdet: Scalable and efficient object detection. 2019.
6. Kaiwen Duan, Song Bai, Lingxi Xie, Honggang Qi, Qingming Huang, and Qi Tian. Centernet: Keypoint triplets for object detection. *Proceedings of the IEEE International Conference on Computer Vision*, 2019-October:6568–6577, 2019.
7. Tsung Yi Lin, Priya Goyal, Ross Girshick, Kaiming He, and Piotr Dollar. Focal loss for dense object detection. *IEEE Transactions on Pattern Analysis and Machine Intelligence*, 42:318–327, 2017.

Mathematical Principles of Password Security

Jorge Loureiro[1], Tiago Pedrosa[2,3], and Maria F. Pacheco[2,3]

[1] Instituto Politécnico Bragança, 5300-253 Bragança, Portugal
jorge.loureiro@ipb.pt
[2] Research Center in Digitalization and Intelligent Robotics (CeDRI), Instituto Politécnico de Bragança, Campus de Santa Apolónia, 5300-253 Bragança, Portugal
pedrosa@ipb.pt, pacheco@ipb.pt
[3] Laboratório Associado para a Sustentabilidade e Tecnologia em Regiões de Montanha (SusTEC), Instituto Politécnico de Bragança, Campus de Santa Apolónia, 5300-253 Bragança, Portugal

Abstract. Authentication algorithms use hash functions to secure credentials and verify user identity. Complex passwords are crucial due to rising online attacks. Penetration testing identifies vulnerabilities in cybersecurity. This paper summarizes a study on mathematical principles (graph theory and frequency analysis) to enhance password audit efficiency. It aims to uncover patterns that weaken supposedly strong passwords. Developed tools for faster testing are compared to brute-force methods. The efficiency of a new graph theory-based dictionary creation approach, utilizing GPU acceleration and distributed computing, is evaluated.

Keywords: Cybersecurity · Passwords · Attacks · Combinatorics

1 Introduction

With today's increase in computational power, the ease of gaining access to data, the number of vulnerabilities identified and exploited by entities with malicious purposes, and the increasing number of attacks performed on systems exposed to the internet, complex passwords become a necessity for the user's security.

The research underlying this paper intends to carry out an analysis of the mathematical principles at the core of the development of secure password systems in authentication algorithms.

The goal is to identify and propose effective solutions for executing attacks, with a view to explore more efficient ways to carry out audits of robustness of passwords, by developing and/or improving existing solutions of password attacks, making them more effective in generating word dictionaries or executing brute-force based attack vectors.

An analysis on the topic of this study will result in greater password security, as it may identify possible patterns that reveal that passwords considered strong are actually much weaker than their users suspect.

2 Context

To understand the fundamental mathematical principles used in password security [1,2], was one of the basis for the proposed problem. However, given the constraints of length, the comprehensive description of those principles utilized in password security had to be sacrificed and, in this paper, the focus has been primarily directed towards highlighting the results drawn from such principles. There are several approaches to brute-force

attacks and dictionary attacks; however, to understand how this process could be accelerated requires a deeper analysis, based on an understanding of the underlying mathematical principles, such as basic counting principles, permutations and combinations of the elements of a set, arrangements with and without repetition, basic models for distributions and frequency, the binomial and multinomial theorems, and lexicographic order as well as many concepts and tools from the context of graph theory [3].

Additionally, through the study of existing open-source password attack solutions, patterns and algorithms commonly used in brute-force and dictionary attacks can be identified. Through the bibliographic review that was carried out, it was discovered a lack of solutions relying on graph theory techniques in order to generate more efficient password dictionaries and perform brute-force attacks. Using the previously performed analysis of open-source attack tools against passwords, a solution was developed to generate password dictionaries combining frequency analysis and graph theory. Through this approach, the dictionary and brute-force attacks efficiency has been improved, and the amount of resources and time required by these methods have been reduced. In order to optimize and accelerate the generation of passwords the use of multiprocessing and multithreading functions, as well as resorting to GPU acceleration [4] in order to traverse all possible paths between two vertices with a predetermined length, are currently being implemented. Through this method it is possible to have a drastic performance improvement, and it is expected that the implementation of parallel computing [5] in order to divide the computational load between multiple machines, will allow an additional reduction of the generation time on a far larger scale.

The results obtained so far are promising, and the developments already attained are currently being used as base for a more targeted study of the Portuguese cyberspace.

3 Results

The following results were generated using an AMD Ryzen 5 5600G processor with 12 cores, 3.9GHz base clock and an Nvidia GeForce RTX 3060 12 GB edition. A frequency analysis of alphanumeric characters from the Rockyou wordlist [6] was performed, analyzing 92.9% of the total number of passwords, equivalent to 13.326.594 entries. From this analysis, several dictionaries with different word sizes were generated using techniques from graph theory. In order to compare the results obtained, dictionaries were also generated using crunch [7], with the same list of characters used to carry out the frequency analysis.

abcdefghijklmnopqrstuvwxyzABCDEFGHIJKLMNOPQRSTUVWXYZ0123456789

Table 1 shows the generation time of these dictionaries, their size and the number of words created. In order to track the execution time for both strategies, the Linux time command was used.

The results in Table 1 show that the execution time is much higher when compared to solutions like crunch; nevertheless, the number of generated passwords is lower. We are convinced that passwords generated through the new strategy are the most probable to be used due to the frequency analysis performed and the use of graph theory to understand relations between characters, resulting in a faster and better-optimized attack execution.

Table 1: Results of dictionary generation.

	Password Length	Time (HH:MM:SS.MS)	File Size (Bytes)	Words
Crunch	2	00:00:03.01	11532	3844
	3	00:00:03.02	953312	238.328
	5	00:00:03.88	73.89×10^6	14.776.336
	5	00:00:59.98	5.49×10^9	916.132.832
	6	00:59:11.75	379.182×10^9	56.800.235.584
Graph Theory	2	00:00:02.44	9230	3150
	3	00:00:02.80	633340	162.136
	4	00:00:10.17	$39{,}09\times10^6$	8.198.020
	5	00:06:54.27	2.27×10^9	406.901.232
	6	10:01:22.07	129.2×10^9	19.818.313.344

4 Conclusion

This paper summarizes a study on mathematical principles, primarily based on graph theory and frequency analysis, to enhance the efficiency of robustness audits on passwords. The objective is to identify patterns that expose supposedly strong passwords as weaker than the users perceive.

Based on the findings, various tools were developed to expedite password testing. The adequacy, speed, and test coverage of these tools will be compared to brute-force methods without the optimizations implemented.

Additionally, a comparison was made between traditional dictionary creation methods based on lexicographic order and the new approach, allowing the evaluation of the efficiency of the proposed method.

GPU acceleration and distributed computing serve as foundational elements to optimize and expedite dictionary creation using graph theory.

References

1. P. Goethals, N. Scala, and D. Bennet. *Mathematics in Cyber Research.* Chapman & Hall, 2022.
2. L. Metcalf and W. Casey. *Cybersecurity and Applied Mathematics.* Syngress Publisher, 2016.
3. A. Tucker. *Applied Combinatorics.* J. Wiley and Sons, 2012.
4. Anaconda. Numba, 2018.
5. Anaconda. Dask, 2018.
6. Brannondorsey. Rockyou.txt, 2017.
7. Jim3ma. Crunch, 2022.

Correlating Sales Amount with Employee Job Satisfaction in the Retail Sector

Lucas D. Borges[1], Inês Sena[1], Felipe G. Silva[1], Florbela P. Fernandes[1,2], Maria F. Pacheco[1,2], Clara B. Vaz[1,2], José Lima[1,2], and Ana I. Pereira[1,2]

[1] Research Center in Digitalization and Intelligent Robotics (CeDRI), Instituto Politécnico de Bragança, Campus de Santa Apolónia, 5300-253, Bragança, Portugal

[2] Laboratório Associado para a Sustentabilidade e Tecnologia em Regiões de Montanha (SusTEC), Instituto Politécnico de Bragança, Campus de Santa Apolónia, 5300-253, Bragança, Portugal

{lucasborges, ines.sena, gimenez, fflor, pacheco, clvaz, jllima, apereira}@ipb.pt

Abstract. This study examines the relationship between employee satisfaction and sales volume in a Portuguese retail store. Pearson's correlation analysis is used, initially indicating no significant relationship. However, in order to explore potential lag effects, cross-correlation analysis was conducted, revealing a weak correlation coefficient of -0.290 with a 7-day delay. These findings will guide future research in understanding the factors that influence the relationship. Further investigation is ongoing to explore the dynamics between employee satisfaction and sales volume in the Portuguese retail industry.

Keywords: Retail sector · Employee satisfaction · Sales amount · Correlation analysis

1 Introduction

Employee satisfaction plays a critical role in the success of any organization. Satisfied employees tend to be more productive, improving overall company performance [1], maximizing profits [2]. This study aims to investigate whether there is a relationship between the value of store sales and employees' satisfaction in the work environment or if an inverse correlation exists. To accomplish this, Pearson's correlation and cross-correlation analyses were used to analyze the relationship between these variables. Data related to employee satisfaction was collected through a web-based questionnaire, while the company provided the data on store sales.

The structure of this paper is as follows: Section 2 describes the data acquisition process and the analytical methods employed. In Section 3, the obtained results are presented. Finally, Section 4 concludes the study by enumerating possible directions for future research.

2 Methodology

A web-based questionnaire was administered using a tablet, consisting of 12 questions on stress level, workload, physical exertion, fatigue, and feeling safe in the work environment. When an employee volunteered to answer, one of the questions was randomly selected for them to answer between "great," "good," "bad," or "terrible," corresponding to scores of +1, +0.5, -0.5, and -1, respectively. The daily score was determined by averaging all responses recorded on the day. Data collection occurred at a Portuguese

retail store between December 10, 2021, and March 21, 2022, totaling 1480 responses in 102 days.

The study relied on sales data provided by the company during the questionnaire period. Pearson's correlation coefficient was initially calculated to assess the relationship between the employee satisfaction index and sales value. The coefficient measures the linear relationship between continuous quantitative variables. Absolute values between 0 and 0.5 indicate weak correlation, while values between 0.5 and 0.8 indicate moderate correlation, and values above 0.8 indicate strong correlation [3].

Next, the cross-correlation coefficient was calculated with a delay of 30 days. This analysis compares the two variables by shifting one series in time and calculating the correlation between corresponding values [4]. The objective was to investigate whether changes in sales value on one day impacted employee satisfaction in subsequent days or vice versa.

3 Results

Pearson's correlation coefficient between the variables is -0.047 and p value is 0.637, indicating a not statistically significant correlation. Fig. 1 presents analysed data over time, where the employee satisfaction score is on the main vertical axis (left) while the sales amount is on the secondary vertical axis (right).

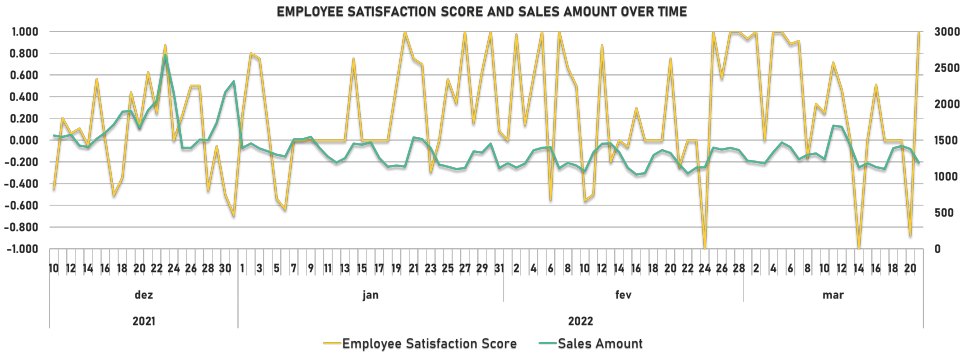

Fig. 1: Evolution of employee satisfaction score and sales amount over time

Given non-significant correlation, a cross-correlation analysis was conducted to ascertain whether one variable affects the other with a lag.

Fig. 2 presents the cross-correlation between the variables.

The highest correlation values occur with delays equal to 7, 8 and 9 days with p-values equal to 0.004, 0.005 and 0.012, respectively. This indicates that sales volume is able to negatively affect employee satisfaction with around a week's delay as the correlation is statistically significant, although it is still weak.

Fig. 2: Cross-correlation between employee satisfaction score and sales amount

4 Conclusion and future works

The correlation between the variables is nearly zero. However, using cross-correlation analysis, a negative impact of sales value on employee satisfaction was observed with a delay of 7 days, although with a weak correlation. Therefore, further investigations will be conducted across multiple stores of the same company to assess potential variations between them, considering a longer time period. Additionally, the quality of the employee satisfaction survey questions will be evaluated to determine if any questions can be eliminated or replaced to enhance the study's effectiveness.

Acknowledgement

The authors are grateful to the Foundation for Science and Technology (FCT, Portugal) for financial support through national funds FCT/MCTES (PIDDAC) to CeDRI (UIDB/05757/2020 and UIDP/05757/2020) and SusTEC (LA/P/0007/2021). This work has been supported by NORTE-01-0247-FEDER-072598 iSafety: Intelligent system for occupational safety and well-being in the retail sector.

References

1. Clement Bellet, Jan-Emmanuel De Neve, and George Ward. Does employee happiness have an impact on productivity? *Saïd Business School WP*, 13, 2019.
2. Metin Bayram, Mustafa C Ünğan, and Kadir Ardıç. The relationships between ohs prevention costs, safety performance, employee satisfaction and accident costs. *International journal of occupational safety and ergonomics*, 23(2):285–296, 2017.
3. Roxy Peck and Jay L Devore. *Statistics: The exploration & analysis of data*. Cengage Learning, 2011.
4. Robert H Shumway, David S Stoffer, and David S Stoffer. *Time series analysis and its applications*, volume 3. Springer, 2000.

Effects of Intensification on Reward Function in Robotic Reinforcement Learning for Digital Twins

Ricardo N. C. Rodrigues[1,2,3], Jaime Fonseca[3], and António H.J. Moreira[1,2]

[1] 2Ai – School of Technology, IPCA, Barcelos, Portugal
[2] LASI – Associate Laboratory of Intelligent Systems, Guimarães, Portugal
[3] Algoritmi Center, University of Minho, Guimarães, Portugal
rnrodrigues@ipca.pt jaime@dei.uminho.pt amoreira@ipca.pt

Abstract. The need for faster, flexible, efficient, and more autonomous production methods created the concept of Industry 4.0, which contains the idea of simultaneously managing the physical assets and their digital duplicate, a Digital Twin (DT). To increase the outputs of this kind of systems, two of the core assets are robotics and Artificial Intelligence (AI) due to their versatility, enabling the systems to adapt to multiple circumstances. One of many sub-subjects of AI is Reinforcement learning that allows the learning of one task by experience. In order to accomplish this, an adequate reward function needs to be set during training. This project aims to evaluate different reward methods (Euclidean distance minimization, Euclidean distance minimization with encouragement and just encouragement) to reduce the distance between the tool in an industrial robotic arm and a specific location. The evaluation of these methods, the minimum distance after training and the time/number of iterations needed to attain such distance will be observed between two distinct training periods (30 minutes and 60 minutes).

Keywords: Digital Twin · Reinforcement Learning · Robotics.

1 Introduction

There are multiple discussion about the definition of DTs (some defines the by the time of creation, some by their functionality, hierarchy, etc.), although their usage brings multiple advantages as: i) increased speed on prototyping and design; ii) waste reduction; iii) reduced maintenance periods; iv) increased performance; v) etc [3].

AI as given proves in various fields, specially Deep Learning (DL) that consists in networks of artificial neurons each one computing information and passing it through to another, inside the concept of DL exists the subject of Reinforcement Learning (RL) where the systems learn by experience, testing and looking at the rewards generated, trying to optimize the outcomes [2] [1].

2 Project overview

This project consists on the creation of a virtual environment in the platform Omniverse Isaac SIM by NVIDIA that provides an environment needed for simulation and multiple content to work with, the contents of the system are the following an industrial robotic manipulator the UR3 from Universal Robots with gripper 2f-85 from Robotiq, the objective of the implemented system is moving the tool to a specific location in the minimum amount of time.

To the system represented in Fig. 1, the reward function will be adjusted in three different approaches.

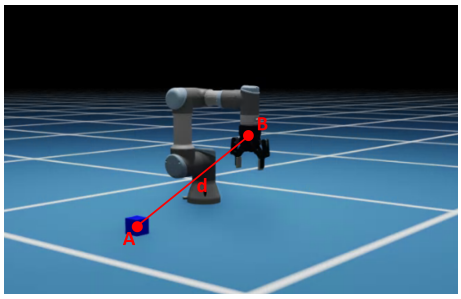

Fig. 1: Example of the system proposed where: A- Cube representing the final location; B- The tool of the robot; d- Distance between the tool and the final location

– Euclidean Distance, using the length of a line segment between the two points (d) is subtracted to the value one, increasing the reward when the distance is shortened.
– Just encouragement, in this function the system is provided with a positive reward (plus one) every time it manages to reduce the Euclidean distance after every action.
– Euclidean Distance plus encouragement, is the fusion of two previous methods.

3 Validation

To validate the experiments and analyze the effects of the different approaches, three main metrics were selected the accuracy of the system (the distance between the tool and the target position), the time after training that it takes to reach the target position and the time/number of iterations the system needs to learn to reach the target as showed at Fig. 2.

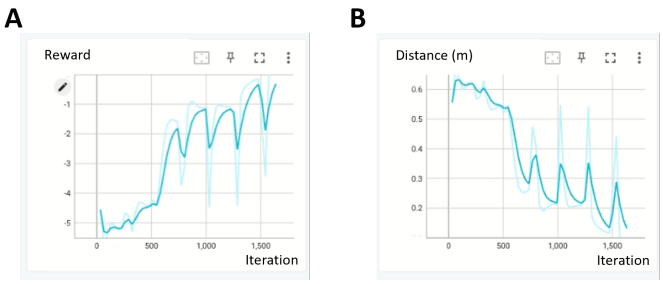

Fig. 2: Example of the information/metrics used to evaluate the approaches. A- Reward values/number of iterations; B- Euclidean Distance (m)/ number of iterations

4 Conclusions

Defining a good reward function is crucial to obtain a reliable system, so a study on different approaches to do it is important. This project is intended to do such a study by validating the effect of different types of reward functions on the simple robotic application to move the robot tool to a determined position.

Acknowledgments

This paper was partially funded by national funds (PIDDAC), through the Portuguese Foundation for Science and Technology – FCT and FCT/MCTES under the scope of the projects UIDB/05549/2020 and UIDP/05549/2020 and under the scope of the project LASI-LA/P/0104/2020. It was also funded with National funding by FCT, through the individual research grant UI/BD/151296/2021.

References

1. Arulkumaran, K., Deisenroth, M.P., Brundage, M., Bharath, A.A.: Deep reinforcement learning: A brief survey. IEEE Signal Processing Magazine **34**, 26–38 (11 2017). https://doi.org/10.1109/MSP.2017.2743240
2. Ibarz, J., Tan, J., Finn, C., Kalakrishnan, M., Pastor, P., Levine, S.: How to train your robot with deep reinforcement learning; lessons we've learned (2 2021). https://doi.org/10.1177/0278364920987859, `http://arxiv.org/abs/2102.02915http://dx.doi.org/10.1177/0278364920987859`
3. Sharma, A., Kosasih, E., Zhang, J., Brintrup, A., Calinescu, A.: Digital twins: State of the art theory and practice, challenges, and open research questions. Journal of Industrial Information Integration **30** (11 2022). https://doi.org/10.1016/j.jii.2022.100383

Segmentation in medical images using a convolutional neural network and dual consistency loss

Helena R. Torres[1,2], Bruno Oliveira[1,2], Pedro Morais[1], Jaime C. Fonseca[2], and João L. Vilaça[1]

[1] 2Ai – School of Technology, IPCA, Barcelos, Portugal
htorres@ipca.pt,boliveira@ipca.pt,pmorais@ipca.pt,jvilaca@ipca.pt
[2] Algoritmi Center, School of Engineering, University of Minho, Guimar˜aes, Portugal
jaime@dei.uminho.pt

Abstract. Medical image segmentation is an important task for several clinical applications. In this work, a U-shaped Convolutional Neural Networks (CNN) architecture is proposed for medical image segmentation. The network generates pixel-wise segmentation and probabilistic contour maps to achieve accurate segmentations. Moreover, a dual consistency loss that relates the two outputs of the network is used. Thus, the network is enforced to consistently learn the segmentation and contour delineation tasks during the training. The proposed method was applied and validated on a public dataset of cardiac 3D ultrasound images of the left ventricle. The results obtained showed the good performance of the proposed method and its applicability for the cardiac dataset, showing its potential to be used in clinical practice for medical image segmentation.

Keywords: Convolutional neural networks · dual consistency loss · image segmentation · cardiac ultrasound.

1 Introduction

Image segmentation is essential for several clinical tasks [1], [2]. However, manual medical image segmentation is a challenging task. Thus, automatic methods can be helpful to design an effective segmentation approach. Currently, the development of such automatic methods was boosted due to the advances of deep learning (DL), particularly Convolutional Neural Networks (CNNs). However, challenges in the current DL-based segmentation approaches can be still identified, such as the accuracy of the delineation near the object's boundaries. In this work, a contour-aware CNN is proposed for the task of medical image segmentation. Specifically, a U-shaped network architecture is applied to predict segmentation and probabilistic contour maps simultaneously. Moreover, to ensure the consistent learning between both predictions, a dual consistency loss is used to explore the intrinsic relation between them.

2 Methods

2.1 Segmentation and contour learning network

A U-shaped encoder-decoder network based on the well-known U-Net [3] is adapted is this work to predict pixel-wise segmentation and probabilistic contour maps simultaneously (Figure 1). Thus, two outputs are extracted from the network, namely: 1) a pixel-wise segmentation; and 2) a contour map.

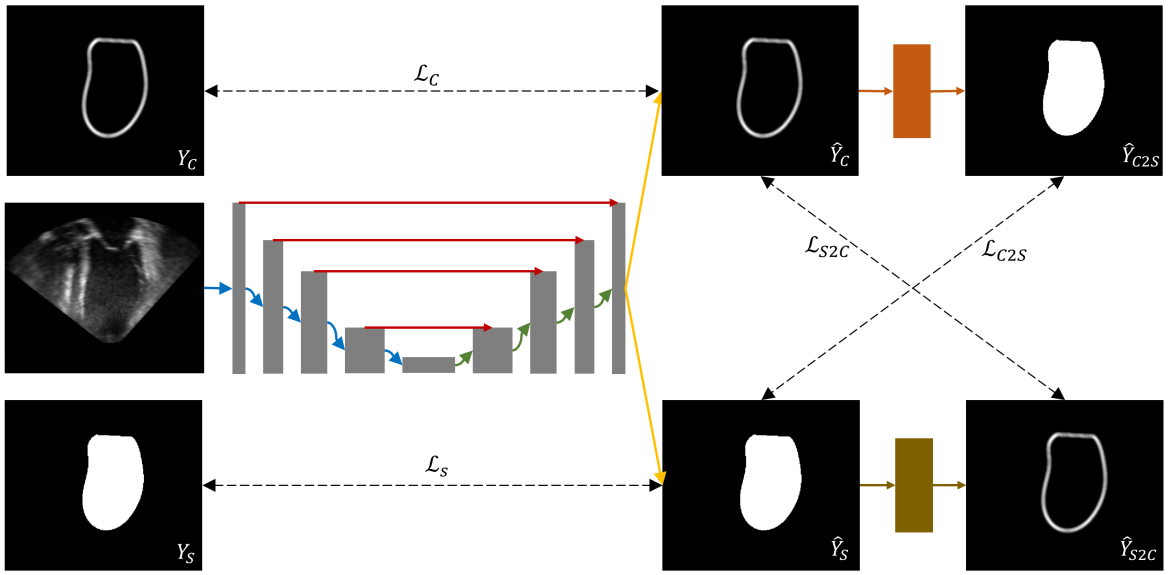

Fig. 1: Overview of the proposed contour-aware network with dual consistency.

The contour probability map is represented by a gaussian-like curve defined around the contour of the object to be segmented. Both network outputs are extracted after application of a Sigmoid activation layer at the end of the network. To guide the network to predict the maps, two different loss functions are used. For the pixel-wise segmentation prediction, the Dice loss function was used to compare the ground-truth segmentation with the predicted segmentation map. For contour prediction, the mean squared error (MSE) loss was applied to accomplish a regression-based task.

2.2 Dual consistent learning

Since the pixel-wise segmentations and the contour maps are explicitly related, a consistency learning between the two outputs of the network must be ensured. To achieve this goal, a dual consistency learning scheme is applied in this work, where the duality is achieved by establishing segmentation-to-contour (S2C) and contour-to-segmentation (C2S) consistencies.

The S2C consistency is achieved by forcing the segmentation output to have a probabilistic contour map similar to the one generated by the network. To compute this consistency, a contour map of the predicted segmentation map is firstly generated. After this, the MSE loss function is applied between the generated contour map and the one predicted by the network. To promote the C2S consistency, the region enclosed by the contour map generated by the network must be coherent with the segmentation output, i.e., must correspond to the same region. Thus, to compute the C2S consistency, a segmentation mask was retrieved from the predicted contour map. Afterward, the Dice loss function is applied between the generated segmentation map and the one predicted by the network. The overall loss is given by the sum of the individual losses.

3 Results

The proposed method was evaluated for the task of left ventricle segmentation in 3D US images, using the CETUS dataset. This dataset is composed of 3D images from 45 subjects (15 training and 30 testing).

The proposed method achieved a mean Dice coefficient of 92.3 $\pm$ 2.3 and a mean average symmetric distance of 1.49 $\pm$ 0.41 mm. These results demonstrate the accuracy of the proposed approach. Figure 2 presents examples of segmentation results.

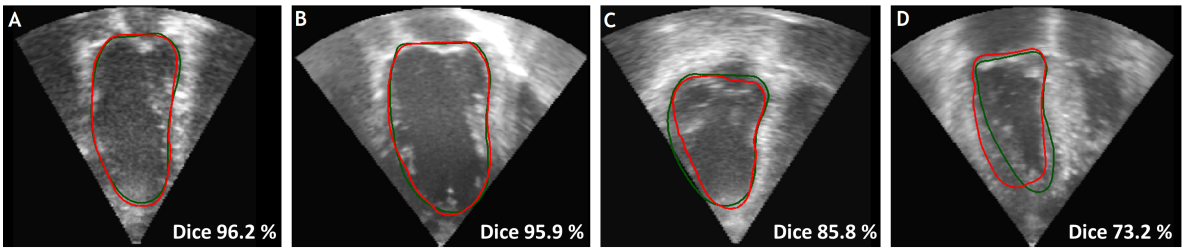

Fig. 2: Example of segmentation results (red) and respective ground-truth (green).

References

1. Torres, H.R., Queiros, S., Morais, P., Oliveira, B., Fonseca, J.C., Vilaca, J.L.: Kidney segmentation in ultrasound, magnetic resonance and computed tomography images: A systematic review. CMPB **157**, 49–67 (2018)
2. Torres, H.R., Morais, P., Oliveira, B., Birdir, C., Rüdiger, M., Fonseca, J.C., Vilaça, J.L.: A review of image processing methods for fetal head and brain analysis in ultrasound images. CMPB p. 106629 (2022)
3. Ronneberger, O., Fischer, P., Brox, T.: U-net: Convolutional networks for biomedical image segmentation. In: Medical Image Computing and Computer-Assisted Intervention–MICCAI 2015: 18th International Conference, Munich, Germany, October 5-9, 2015, Proceedings, Part III 18. pp. 234–241. Springer (2015)

New Interventional Framework for the Planning of Left Atrial Appendage Occlusion in 2D Ultrasound Imaging

Rafael Fernandes[1], Pedro Morais[1], and João Vilaça[1]

2AI - School of Tecnology, IPCA, Barcelos, Portugal
jrfernandes@ipca.pt, pmorais@ipca.pt, jvilaca@ipca.pt

Abstract. Left atrial appendage (LAA) is the major source of thromboembolism in patients with non-valvular atrial fibrillation. Currently, LAA occlusion can be offered as a treatment for these patients, obstructing the LAA through a percutaneously delivered device. Nevertheless, correct device sizing is a complex task, requiring manual analysis of medical images. This approach is sub-optimal, time-demanding, and highly variable between experts. Different solutions were proposed to improve intervention planning, but no efficient solution is available to 2D ultrasound, which is the most used imaging modality for intervention planning and guidance. This study will focus on developing new automated artificial intelligence (AI)-based solutions to automatically segment the LAA on 2D ultrasound images and predict the optimal device size for subsequent surgical intervention and incorporate everything into an interface for real-time visualization of the developed methodologies.

Keywords: Deep learning · left atrial appendage segmentation · left atrial appendage occlusion · 2D ultrasound image

1 Introduction

The left atrial appendage (LAA) is a finger-like projection from the main body of the left atrial (LA). The junction is well-defined by a narrowing in the appendage orifice [1]. Recent studies indicate that it is the source of thromboembolism in approximately 90% of patients presenting with non-valvular atrial fibrillation (NVAF). Thus, percutaneous LAA occlusion is presented as a solution to reduce the risk of thromboembolic events [2]. This small and little invasive cardiac intervention aims to close the LAA orifice by placing the device that seals the connecting orifice between LA and the LAA. Closure devices are available in several predefined sizes, for each patient, an appropriately sized device must be selected. The implementation of the respective device requires a pre-analysis through echocardiography or another imaging method such as, Computed tomography angiography (CT) where the largest landing zone is measured for the sizing of the device. Currently, there are some techniques for LAA segmentation using 3D models, simple image-based techniques [3], deformable models [4], or even the use of machine learning [5]. Segmentation techniques have also been explored from 3D-TEE images, using deformable method [6]. One of the aspects that we have not seen in any study is the segmentation of LAA in 2D-TEE images, which is still one of the most used imaging modalities for screening and training. This type is more used due to the ease of visualization and comprehension of the data compared to 3D. Thus concluding that as the central objective of this research: - Build a framework capable of automatically performing all the processes regarding the occlusion plan of the LAA. As important steps in the study, the first step will be to develop a 2D ultrasound segmentation strategy using state-of-the-art neural networks and conclude which is the best

neural network for the segmentation of the LAA. The second step will be to develop a strategy to extract the clinical indicators using state-of-the-art neural networks and to evaluate them in order to select the best strategy. all AI modules will be directly embedded in an interface for real-time visualization of the developed methodologies, developed using GE's Developer Partnership Program, which allows running the software directly on the ultrasound machine. Validation will be done on a Phantom model, creating different Phantoms with different implants, and we want to see the segmentation working in real time and verify that the measurements are correct. Also validate the framework in terms of computational power (i.e. frame-rate, latency) and request tests with clinicians to evaluate the developed system.

2 Results

For the development of the proposed two-dimensional segmentation methods it was necessary to prepare a dataset with 2D ultrasound images these were taken from 3D slices of a Transesophageal echocardiography (TEE) dataset, then it was also collected some images from the ultrasound internet referring to the LAA, then it was performed all image pre processing. After the dataset was created, we conducted a search to select the neural networks that could bring the best results and did a comparative study with the following selected networks: Unet, UnetR, AttUnet, TransAttUnet. All networks chosen are based on UNET since it is the network with the best benchmark for segmentation in medical images the figure 1 represent the network architecture under study.

Table 1: QUANTITATIVE COMPARISON OF THE DIFFERENT METHODS

Network	Evaluation Metrics						
	DC[a]	Acc[b]	Rec[c]	Spe[d]	Pre[e]	HD95[f]	Assd[g]
Unet	88.3±4.21	98.96±0.44	86.46±7.65	99.28±0.27	**91.0±5.69**	4.94±5.69	1.42±0.52
UnetR	87.6±4.39	98.94±0.46	89.78±6.99	99.22±0.44	86.22±6.94	5.01±2.21	1.61±0.91
AttUnet	88.26±3.49	99.00±0.45	89.78±6.21	**99.45±0.37**	88.25±7.30	**4.66±1.71**	1.31±0.41
TransAttUnet	**89.2±4.37**	**99.09±0.46**	**93.09±5.93**	99.37±0.42	86.30±7.79	4.85±2.05	**1.30±0.58**

[a]Dice metri, [b]Acurracy, [c]Recall, [d]Specifity, [e]Precision, [f]Hausdorf Distance, [g]Average symmetric surface distance

As illustrated in table 1 and figure 2 we have the results in our study, in a generic way, the obtained results demonstrated that the current state-of-the-art networks achieved satisfactory results for this segmentation task however to get better accuracy new ways

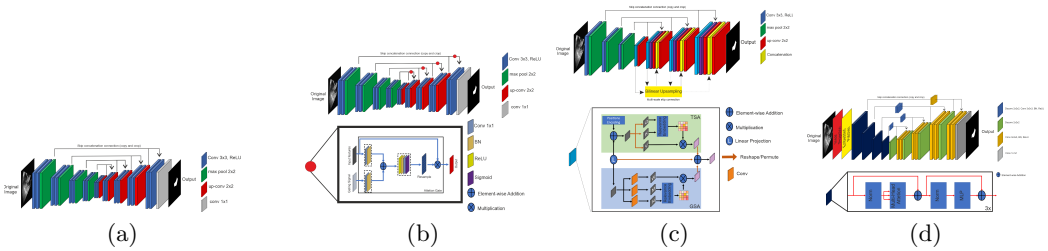

(a) (b) (c) (d)

Fig. 1: Neural network architecture: a) Unet b) UnetR c) AttUnet d) TransAttUnet

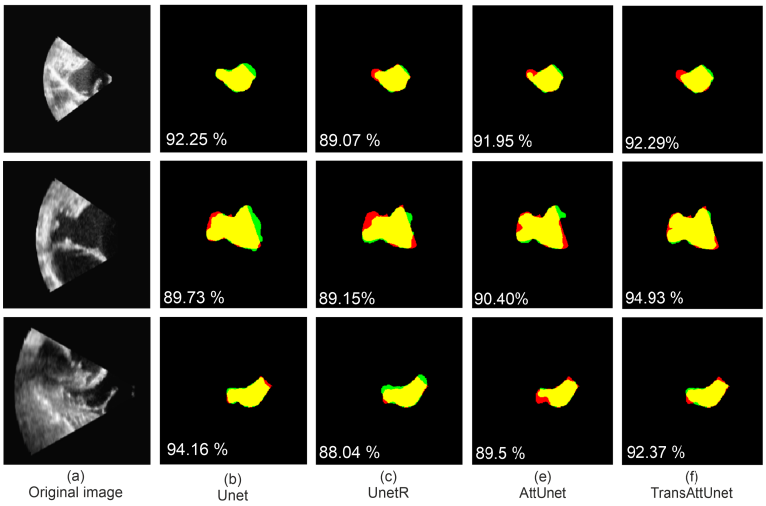

Fig. 2: Results of the different methods trained, in the first column the original image and the remaining columns are the resulting masks for each network, the yellow color represents the intersection of the predict with the ground truth, the green color represents the predict of the network and red the ground truth

to optimize neural networks are being tested, such as better approaches for loss functions and other hyper parameters, which may allow, in real-time, the enhancement of the LAA segmentation into the US image throughout the intervention, ultimately easing the identification of the relevant structure, as well as, simplifying the extraction of relevant indexes.

Acknowledgments

This project was funded by the projects "NORTE-01-0145-FEDER-000045" and "NORTE-01-0145-FEDER-000059", supported by Northern Portugal Regional Operational Programme (Norte2020), under the Portugal 2020 Partnership Agreement, through the European Regional Development Fund (ERDF). It was also financed by national funds, through FCT - Foundation for Science and Technology and FCT / MCTES under the project UIDB / 05549/2020, UIDP/05549/2020, CEECINST/00039/2021 and LASI-LA/P/0104/2020. This project was also funded by the Innovation Pact HfFP – Health From Portugal, co-funded from the "Mobilizing Agendas for Business Innovation" of the "Next Generation EU" program of Component 5 of the Recovery and Resilience Plan (RRP), concerning "Capitalization and Business Innovation", under the Regulation of the Incentive System "Agendas for Business Innovation".

References

1. Beigel, Roy and Wunderlich, Nina C and Ho, Siew Yen and Arsanjani, Reza and Siegel, Robert J, The left atrial appendage: anatomy, function, and noninvasive evaluation. JACC: Cardiovascular imaging, 2014.
2. Basu Ray, Indranill and Khanra, Dibbendhu and Shah, Sumit and Char, Sudhanva and Jia, Xiaoming and Lam, Wilson and Mathuria, Nilesh and Razavi, Mehdi and Jain, Bhavna and Lakkireddy, Dhanunjaya and others, Meta-analysis comparing WatchmanTM and Amplatzer devices for stroke prevention in atrial fibrillation. Frontiers in cardiovascular medicine, 2020.
3. Song, Hongning and Zhou, Qing and Deng, Qing and Chen, Jinling and Zhang, Lan and Tan, Tuantuan and Guo, Ruiqiang, Morphologic assessment of the left atrial appendage in patients with atrial fibrillation by gray values–inverted volume-rendered imaging of three-dimensional transesophageal echocardiography: A comparative study with computed tomography. Journal of the American Society of Echocardiography, 2016.

4. Pedro Morais and Dominik Nelles and Jan Wilko Schrickel and Georg Nickenig and Jan D'hooge and Alexander Sedaghat and João L. Vilaça, 3D segmentation of the left atrial appendage in computed tomography for planning of transcatheter occlusion. Medical Imaging 2022: Image-Guided Procedures, Robotic Interventions, and Modeling, in SPIE. 2022.
5. Wang, Lei and Feng, Jianjiang and Jin, Cheng and Lu, Jiwen and Zhou, Jie, Left atrial appendage segmentation based on ranking 2-D segmentation proposals. Statistical Atlases and Computational Models of the Heart. Imaging and Modelling Challenges: 7th International Workshop, STACOM 2016, Held in Conjunction with MICCAI 2016, Athens, Greece, October 17, 2016, Revised Selected Papers 7, 2017.
6. Morais, Pedro and Vilaça, João L. and Queirós, Sandro and De Meester, Pieter and Budts, Werner and Tavares, João Manuel R. S. and D'Hooge, Jan, Semiautomatic Estimation of Device Size for Left Atrial Appendage Occlusion in 3-D TEE Images. IEEE Transactions on Ultrasonics, Ferroelectrics, and Frequency Control, 2019.

Effect of Dielectric Material Geometry on Mechanical Deformation of Capacitive Sensors for Compressing Force Measurement

Ricardo Rodrigues[1,2], Daniel Miranda[1,2], and João Vilaça[1,2]

[1] 2Ai - School of Technology, IPCA, Barcelos, Portugal
[2] LASI, Associate Laboratory of Intelligent Systems, Guimarães, Portugal
rmrodrigues@ipca.pt, damiranda@ipca.pt, jvilaca@ipca.pt

Abstract. The integration of sensors in devices can extend life expectancy and improve quality of life. Sensors can be used for diagnosis, prevention and treatment of users, as well as to assess performance and fitness of athletes or in contexts of postural control. Computational simulations were used to optimize the sensor geometry, select dielectric materials, and position the sensors in monitoring devices. An optimization and prediction study was performed on the influence of different dielectric material geometries on mechanical deformation and sensor performance. Five new geometries were proposed, and only three showed significant displacement when a compressive force was applied.

Keywords: Capacitive Sensors · Finite Element Method · Simulation · Sensor Geometries · Dielectric material sensors.

1 Introduction

The development and integration of sensors in devices has the potential to extend life expectancy and enrich the quality of life of the next generation [1]. The development and integration of sensors allows the diagnosis, prevention and treatment of users and can also help in the evaluation of performance and physical condition of athletes [2], like for example measuring the force exerted on your hand when holding an object and in postural control. This study aims to develop and optimize the performance and sensitivity of capacitive sensors that will be applied in devices for monitoring compressive force gradients. Thus, the aim is to optimize and predict the influence of different dielectric material geometries of capacitive sensors with various dielectric materials on mechanical deformation and performance. With the application of a compressive force, a larger displacement between the electrodes had improved the capacitive response. To evaluate the influence of dielectric material geometry on the deformation caused by the application of a compressive force, five new geometries were proposed.

2 Experiences and Results

Were developed, in computer simulations based on the Finite Element Method (FEM), these being a procedure that allows for easier modelling of complex and irregular geometric shapes, to study the influence of different dielectric geometries, with the dimensions 10x10mm, with two different dielectric materials on the mechanical deformation suffered when subjected to the application of a range of compressive forces between

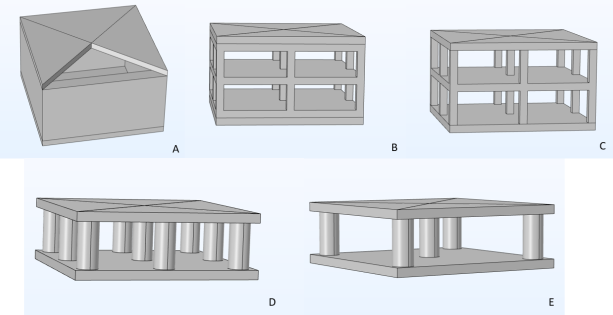

Fig. 1: Proposed dielectric material geometries for capacitive sensors.

(0.1N to 5N). The proposed geometries to be studied are illustrated in Figure1.

The simulations developed were applied to the Linear Elastic mechanical model and a stationary study. The materials that were used in tests were Natural Rubber (NR) and Silicone rubber (SIR). The mechanical parameters of the dielectric materials used in the simulations, such as Young's modulus, Poisson's ratio and Density are illustrated in Table 1.

Table 1: Mechanical parameters of dielectric materials applied in the simulations.

Material	**Young's Modulus**	**Poisson's ratio**	**Density**
Natural Rubber	$5x10^6$ Pa	0.45	1320 Kg/m^3
Silicone rubber	$8x10^6$ Pa	0.495	1200 Kg/m^3

To determine the best geometries, we present the compressive strain values obtained by applying forces ranging from 0.1 N to 5 N to various dielectric material geometries for the two selected materials.

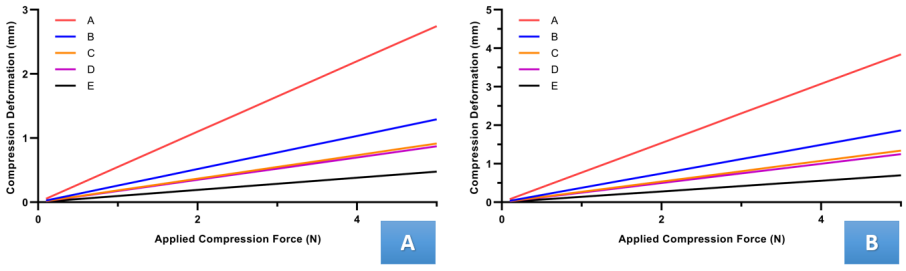

Fig. 2: Compression displacement as a function of the compression force applied to several dielectric material geometries proposed for different dielectric materials: A) NR and B) SIR.

Based on Figure 2, we concluded that the geometries with the best performance and highest compression strains were "A", "B", and "C". Among these three geometries, "A" exhibited higher performance in terms of both high compressive and overall deformation across all three dielectric materials, which implies a higher capacitive sensor response.
The Figure 3 illustrates the pressure gradient and strain experienced by the "A" geometry with the SIR (silicone rubber) dielectric material under applied compressive forces of 0.5 N and 5 N. As shown in Fig 3, silicone rubber (SIR) is the dielectric material

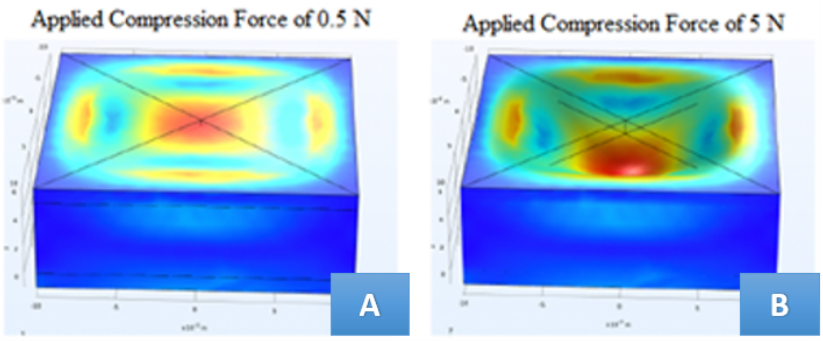

Fig. 3: Pressure gradient and strain obtained by the "I" geometry with the SIR dielectric material under applied compressive forces: A) 0.5 N and B) 5 N

with the highest ease of compression deformation, which implies a better performance and response of the capacitive sensor to be applied in monitoring technologies that aim to measure low intensity compressive forces. The next step will be to increase the area of the sensor plates to cause an increase in the capacitance variation.

3 Acknowledgments

This work was funded by the project "NORTE-01-0145-FEDER-000045", supported by Northern Portugal Regional Operational Programme (Norte2020), under the Portugal 2020 Partnership Agreement, through the European Regional Development Fund (ERDF). It was also funded by national funds (PIDDAC), through the FCT – Fundação para a Ciência e a Tecnologia and FCT/MCTES under the scope of the projects UIDB/05549/2020, UIDP/05549/2020 and LASI-LA/P/0104/2020.

References

1. Broadbent, E., Stafford, R., Macdonald, B.: Acceptance of healthcare robots for the older population: Review and future directions. I. J. Social Robotics **1**, 319–330 (11 2009). https://doi.org/10.1007/s12369-009-0030-6
2. De Fazio, R., Mastronardi, V.M., De Vittorio, M., Visconti, P.: Wearable sensors and smart devices to monitor rehabilitation parameters and sports performance: An overview. Sensors **23**(4) (2023). https://doi.org/10.3390/s23041856, `https://www.mdpi.com/1424-8220/23/4/1856`

Thermal-Based Nutritional Recommendations: AquaVitae System

Henrique S. Marcuzzo[1,3], Maria J. V. Pereira[1,2], Paulo Alves[1,2], and Juliano H. Foleis[3]

[1] Research Center in Digitalization and Intelligent Robotics (CeDRI), Instituto Politécnico de Bragança, Campus de Santa Apolónia, 5300-253, Bragança, Portugal
henrique.marcuzzo@ipb.pt, mjoao@ipb.pt, palves@ipb.pt
[2] Laboratório Associado para a Sustentabilidade e Tecnologia em Regiões de Montanha (SusTEC), Instituto Politécnico de Bragança, Campus de Santa Apolónia, 5300-253, Bragança, Portugal
[3] DACOM, Universidade Tecnológica Federal do Paraná, UTFPR, Brasil
julianofoleiss@utfpr.edu.br

Abstract. In this article, we introduce an innovative recommendation system designed to assist nutritionists in creating personalized and effective nutritional plans for their clients. The system gathers data on user preferences, dietary restrictions, and nutritional needs, providing a variety of meal options tailored to each individual. Continuous diet monitoring of patients and prioritizing thermogenic foods are additional features that enhance efficiency and user experience.

Keywords: Recommendation System · Thermal-Based · Nutritional Plan.

1 Introduction

This paper introduces a recommendation system designed to improve the interaction between nutritionists and patients, offering access to customizable nutritional plans and tracking of meals. As part of the Aquae Vitae Research Project, the system emphasizes thermal-based foods in meal suggestions to foster balanced nutrition.

Our approach to developing this system combines rule-based and scoring methodologies, as informed by key resources [1–3]. This approach takes into account user preferences, dietary restrictions, and nutritional plan rules to generate accurate recommendations.

By selecting this system, we aim to meet the specific needs of the clients while enhancing the overall experience for both patients and nutritionists, leveraging insights from pivotal research in recommendation systems.

2 Development and Tests of the Recommendation System

Our dietary recommendation system creates personalized plans considering user's preferences, consumption history, and nutritional restrictions. The system follows two key steps: food ranking and nutritional plan formulation.

During food ranking, scores are assigned to foods based on user preference, food category, and consumption frequency. For instance, liked foods and those similar to liked ones score higher, while overly-consumed foods score lower to promote dietary variety.

For the nutritional plan formulation, meal types and permitted items are gathered, and meal items are then ranked based on their composite food scores. The meals are divided into three groups according to their scores, with one item from each group chosen for the plan based on the user's nutritional needs.

This system creates diverse and suitable dietary plans tailored to user's needs and preferences. Figure 1 provides a detailed depiction of this recommendation process, from user data analysis to personalized plan generation.

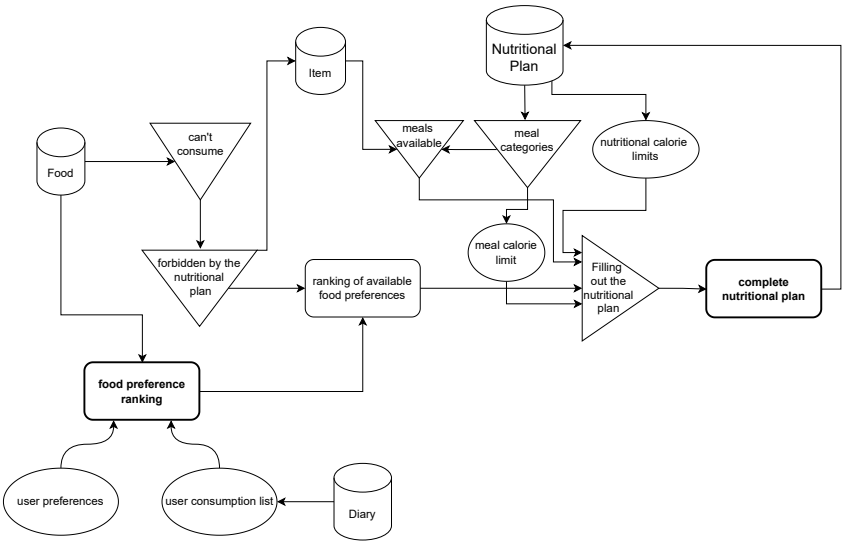

Fig. 1: Recommendation System process overview.

Comprehensive endpoint testing was performed on the complete system, encompassing both the nutritional plan management and recommendation subsystems. These tests confirmed the functionality and performance of the integrated system, achieving an impressive 96% code coverage and maintaining median response times of less than 20 ms.

Additionally, meal plan creation was tested, demonstrating the system's ability to provide varied meal suggestions tailored to user preferences and needs. This adaptability was evident across four different scenarios with varying inputs. Figure 2 illustrates an example of a full day meal plan generated using only daily caloric intake data.

3 Conclusion & Future Work

We developed a recommendation system to aid nutritionists and enhance patients' dietary experiences, showing promising early results. Future plans include system automation for meal importation, leveraging machine learning for improved scoring metrics, and professional validation for aligning recommendations with expert judgement, thereby promoting variety and better catering to user needs.

meal_date	meal_description	meal_start_time	meal_end_time	food_description	amount
2023-04-21	Ao acordar	09:00:00+00	09:30:00+00	Chá de hortelã	0,5
				Limonada com gengibre	0,5
				Suco de melancia com hortelã	0,5
	Pequeno-almoço	10:30:00+00	11:00:00+00	Sanduíche natural com queijo e peito de peru	0,5
				Biscoitos integrais com geleia de frutas sem açúcar e queij	0,5
				Salada de frutas com iogurte e coco ralado	0,5
	Meio da Manhã	11:30:00+00	12:00:00+00	Sanduíche de frango desfiado com cenoura e alface	0,5
				Biscoitos integrais com geleia de frutas sem açúcar e queij	0,5
				Smoothie de morango e banana	0,5
	Almoço	13:00:00+00	14:00:00+00	Sanduíche de pão sírio com pasta de grão-de-bico e legum	1
				Omelete de legumes com macarrão de abobrinha e salada	0,5
				Bife de alcatra ao molho de cogumelos com arroz selvager	0,5
	Lanche da tarde	16:00:00+00	16:30:00+00	Sanduíche integral com atum e salada	0,5
				Salada de grão-de-bico com atum e vegetais	0,5
				Biscoitos integrais com geleia de frutas sem açúcar e queij	0,5
	Jantar	21:00:00+00	22:00:00+00	Tofu grelhado com purê de mandioquinha e brócolis no va	1
				Salada de grão-de-bico com atum e vegetais	1
				Torrada integral com queijo quark e frutas	2,5
	Ceia	23:30:00+00	00:00:00+00	Biscoitos integrais com geleia de frutas sem açúcar e queij	0,5
				Sanduíche integral com atum e salada	0,5
				Bowl de frutas com chia e mel	0,5

Fig. 2: Nutritional plan without any input.

References

1. Kardan, A.A., Ebrahimi, M.: A novel approach to hybrid recommendation systems based on association rules mining for content recommendation in asynchronous discussion groups. Information Sciences **219**, 93–110 (2013)
2. Song, H., Zhang, H., Xing, Z.: Research on personalized recommendation system based on association rules. In: Journal of Physics: Conference Series. vol. 1961, p. 012027. IOP Publishing (2021)
3. Zhang, S., Yao, L., Sun, A., Tay, Y.: Deep learning based recommender system: A survey and new perspectives. ACM Comput. Surv. **52**(1) (February 2019). https://doi.org/10.1145/3285029, `https://doi-org.ez48.periodicos.capes.gov.br/10.1145/3285029`

Joint Classification and Segmentation of Chronic Venous Disorders using Convolutional Neural Networks

Bruno Oliveira[1,2], Helena R. Torres[1,2], Pedro Morais[1], António Baptista[1], Jaime Fonseca[2], and João L. Vilaça[1]

[1] 2Ai – School of Technology, IPCA, Barcelos, Portugal
boliveira@ipca.pt, htorres@ipca.pt, pmorais@ipca.pt, jvilaca@ipca.pt
[2] Algoritmi Center, School of Engineering, University of Minho, Guimarães, Portugal
jaime@dei.uminho.pt

Abstract. Chronic Venous Disorders (CVD) of lower limbs affect a significant portion of the adult population in Europe and North America. As the aging population continues to grow, the burden of CVD and associated healthcare costs are expected to rise. Early diagnosis and effective monitoring are crucial for treatment planning and assessing the progression of CVD. However, the current approach relies on visual recognition by physicians, which is time-consuming and subjective. In this study, we propose a novel automatic strategy called VENet, which combines segmentation and classification using a multi-task deep learning network. By leveraging information from both tasks, VENet improves learning efficiency and performance. Our method was evaluated on a dataset of 1376 CVD images and compared against state-of-the-art strategies. The results demonstrate that VENet achieved high accuracy, precision, and recall of 96.4%, 96.4%, and 97.2% for classification, and 75.4%, 76.7%, and 76.7% for segmentation, respectively. The joint formulation of segmentation and classification outperformed conventional strategies, particularly in segmenting small lesions, highlighting its added value.

Keywords: chronic venous disorders · classification · convolution neural networks · multi-task · segmentation.

1 Introduction

Chronic Venous Disorders (CVD) in the lower limbs are highly prevalent worldwide, accounting for 1-2% of healthcare budgets in Western Europe and North America [1]. Initially, CVD presents symptoms such as leg pain, discomfort, heaviness, and swelling, negatively impacting the patient's skin and overall quality of life. As the disease progresses to varicose veins, edema, skin changes, and ulcers, the quality of life further declines, leading to an increased demand for treatment [2]. Accurate diagnosis is crucial to provide appropriate treatment and manage medical resources due to the diverse signs and symptoms associated with CVD severity. However, current diagnosis protocols rely on physical examination and visual inspection, heavily relying on physician expertise and often resulting in incomplete recognition of CVD signs and undertreated cases [1]. In this work it is proposed a novel DCNN-based framework, VENet, for segmenting and classifying the severity of CVD from medical images. By sharing the same feature map and leveraging high-level features, this approach has the potential to enhance the accuracy of both tasks. VENet provides classification and segmentation results for different lesion severities (telangiectasias and reticular veins, varicose veins, and ulcers).

2 Methods

VENet is based on the U-Net architecture and consists of four parts: the encoding path, classification head, decoding path, and segmentation head (see Fig. 1).

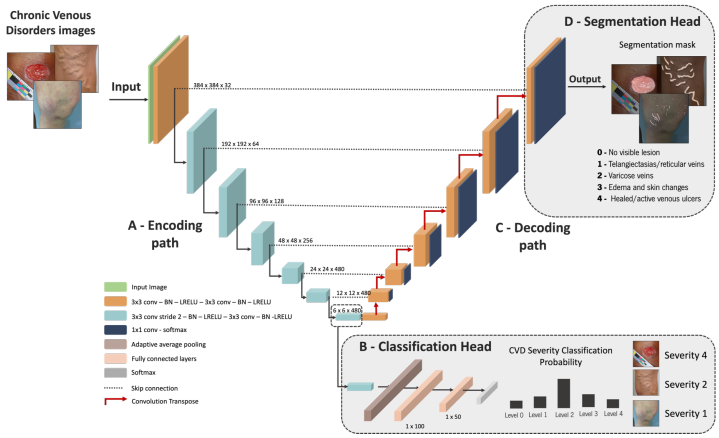

Fig. 1: Overview of the proposed strategy for CVD classification and segmentation.

The encoding path extracts high-level features using downsampling blocks, each composed of two convolutional layers with batch normalization and Leaky ReLU. The classification head, located at the bottom of VENet, utilizes the high-level features for CVD classification, employing convolution and fully connected layers. The decoding path restores feature maps to the original input size using upsampling blocks, with skip connections established between the encoding and decoding paths. The segmentation head takes features from the last decoding block and applies convolution layers with batch normalization and Leaky ReLU to generate instance-level probability maps. Finally, we employ a multi-task loss consisting of a classification and segmentation losses. The classification loss is calculated using multi-class cross-entropy. For the segmentation task, we combine cross-entropy loss with DICE loss. By minimizing the linear combination of both during training, VENet can effectively learn to classify and segment CVD lesions simultaneously.

3 Results

Table 1 provides a comparison of the performance between VENet and other state-of-the-art multi-task DCNNs [3] [4] [5] [6].

For the classification task, two networks presented slightly better results, namely DSI-Net and Che et. al.. Still, no significant differences were obtained. For the segmentation task, statistically significantly better performance was obtained, with an improvement of around 4% of the DICE for the second-best performance. In detail, DSI-Net, Che et al., and MTCSN employed feature passing modules to enhance segmentation performance. To that, VENet established an early connection between the

Table 1: Comparison of the proposed method against other multitask DCNN

Model	Segmentation			Classification			
	DICE	PRE	REC	ACC	PRE	REC	F1-score
Proposed	**75.4±9.6**	76.7±10.1	**76.7±13.3**	96.4	96.4±5.0	97.2±2.6	96.3
Le et. al.	61.7±11$^{\beta}$	62.4±12$^{\beta}$	66.1±16$^{\beta}$	96.4	95.9±5.2	97.1±3.6	96.3
DSI-Net	71.4±11.4$^{\beta}$	**77.2±10.8**	68.7±15.7$^{\beta}$	**97.8**	**97.5±3.3**	**97.9±3.4**	**97.8**
MTCSN	60.8±14.6$^{\beta}$	62.5±14.4$^{\beta}$	64.6±21.2$^{\beta}$	95.6	95.4±3.5	95.9±2.8	95.6
Che et. al.	70.8±10.1$^{\beta}$	73.4±10.7$^{\beta}$	70.5±13.8$^{\beta}$	97.1	96.7±3	97.5±3.4	97.1

$^{\beta}$ $p < 0.05$, Paired t-test against the proposed VENet strategy.
$^{\alpha}$ $p < 0.05$, Two-sided McNemar's test against the proposed VENet strategy.

tasks in the encoding path. This early integration enabled better preservation of spatial details, especially for smaller lesions. These findings confirm the effectiveness of proposed network, mainly in segmenting small anatomical structures. Overall, VENet has offers valuable support to physicians and patients in the diagnosis and monitoring of CVD.

References

1. A. Meesters, L. H. U. Pitassi, V. Campos, A. Wolkerstorfer, and C. C. Dierickx, "Transcutaneous laser treatment of leg veins," Lasers in Medical Science, vol. 29, no. 2, pp. 481–492, Mar. 2014:
2. E. Rabe, J. J. Guex, A. Puskas, A. Scuderi, F. Fernandez Quesada, and VCP Coordinators, "Epidemiology of chronic venous disorders in geographically diverse populations: results from the Vein Consult Program," Int Angiol, vol. 31, no. 2, pp. 105–115, Apr. 2012:
3. M. Zhu, Z. Chen, and Y. Yuan, "DSI-Net: Deep Synergistic Interaction Network for Joint Classification and Segmentation With Endoscope Images," IEEE Trans. Med. Imaging, vol. 40, no. 12, pp. 3315–3325, Dec. 2021:
4. S. Chen, Z. Wang, J. Shi, B. Liu, and N. Yu, "A multi-task framework with feature passing module for skin lesion classification and segmentation," in 2018 IEEE 15th International Symposium on Biomedical Imaging (ISBI 2018), Washington, DC, Apr. 2018, pp. 1126–1129:
5. T.-L.-T. Le, N. Thome, S. Bernard, V. Bismuth, and F. Patoureaux, "Multitask Classification and Segmentation for Cancer Diagnosis in Mammography:
6. Z. Kong et al., "Multi-Task Classification and Segmentation for Explicable Capsule Endoscopy Diagnostics," Front. Mol. Biosci., vol. 8, p. 614277, Aug. 2021:

Infant head shapes with deformational plagiocephaly for training in diagnosis

Fernando Veloso[1], Anne Fritze[2], Helena R. Torres[1], Pedro Morais[1], and João L. Vilaça[1]

[1] 2Ai – School of Technology, IPCA, Barcelos, Portugal
fveloso@ipca.pt
[2] Department for Neonatology and Pediatric Intensive Care, Medical Faculty of TU, Children's Hospital, Dresden, Germany

Abstract. Deformational plagiocephaly is a condition characterized by the asymmetrical shape of an infant's skull. It typically occurs due to external pressures on the soft skull bones, such as prolonged positioning on one side of the head. Treatment options may include repositioning techniques, physical therapy, or in some cases, helmet therapy to help remodel the skull during growth. Early diagnosis is important, as the treatment window is only in the first months of life, while the infant´s skull is malleable and growing fast. However, parents and physicians have difficulty recognizing the early stages of this deformity, unable to prevent the aggravation of the deformity and delaying a possible early treatment with better clinical results. In this work, ten infant head models produced by additive manufacturing for training of physicians are presented, to help them make an earlier identification of possible cases of deformational plagiocephaly. The infant´s head models are produced by additive manufacturing and contain inscribed several measurements that are typical in this kind of diagnosis. During the training, the physicians must perform measurements on a specified section plane of the head and assess the degree of deformity for each head.

Keywords: Deformational plagiocephaly · Diagnosis · Training.

1 Introduction

1.1 Deformational plagiocephaly

Deformational plagiocephaly (DP), also known as positional preference is when an asymmetrical or deformed head shape occurs in infants or newborns. It happens when the soft skull bones are subjected to external pressures or forces that flatten or deform them. DP can be divided in two types: Plagiocephaly, when one side of the skull flattens, the head seems to be shaped like a parallelogram when viewed from above. A pronounced forehead, bulging on the opposite side, and asymmetrical facial characteristics may also be present. Brachycephaly: This condition causes the rear of the skull to flatten out generally, giving rise to a wider and shorter head shape. It often happens as a result of outside influences such persistent pressure on one area of the head, restricted movement in the womb, or spending prolonged periods of time in one position (such as sleeping regularly on the same side).

Early diagnosis is essential because, in addition to cosmetic difficulties connected to the abnormalities, infants with this syndrome may also be subjected to developmental delay [1]. The window for therapy only lasts for the first few months of life, when the baby's skull is moldable and rapidly developing. Parents and doctors, however, sometimes struggle to spot this deformity in its earliest phases, failing to stop the

deformity from getting worse and postponing a potential early therapy that would have superior clinical outcomes. The recognition of head deformities is an expertise mainly acquired by craniofacial specialists and other specialized medical doctors. However, to make this type of knowledge more accessible to other health professionals, some initiatives were taken. For example, to teach medical staff how to analyze head shapes, a serious game for medical training called Head Shape Inspector was developed [2]. A recent work presented a method to identify craniofacial deformities with the help of a smartphone app [3].

2 Methods

In clinical practice, the measurements to diagnose this type of deformities is made by acquiring the head surface either by previously prescribed CT scans, or by a 3d head scan using photogrammetry or other process. In the resulting three-dimensional model, the contour of the infant´s head in a specific plane is analyzed. Definition of the measurement plane (MP) that is frequently used to evaluate skull asymmetries in clinical settings.

The left Tragion (TrL), right Tragion (TrR), and the Sellion landmarks serve as the foundation for the MP, which is constructed from the auxiliary plane (AP). At the maximal cranial length (L), the MP is displaced from the AP. B - MP measures in two dimensions. W is the cranial width, perpendicular to the cranial length, and ED is the ear deviation. Diagonal A (DA) is the longer transcranial diagonal, at an angle of 30 or 40 degrees to the length axis. Diagonal B (DB) is the shorter transcranial diagonal, at an angle of 30 or 40 degrees to the length axis. The difference between the cranial diagonals' absolute values is known as the CVA, and the CVAI is the CVA divided by the longer diagonal times one hundred. As a result, the CVAI measures the CVA in relation to the size of the head as a whole. Ten newborn skull shapes with various degrees of Deformational Plagiocephaly (DP), Brachycephaly, or a combination of the two were obtained from the Department for Neonatology and Pediatric Intensive Care, Children's Hospital, (Medical Faculty of TU Dresden 01307, Germany). A straightforward threshold method was used to semi-automatically segment the heads in the MR images, and mathematical morphology was then used to enhance the results. As a result, the molds' 3D shapes were formed. When necessary, manual alterations of 3D models with incorrect segmentation were made [4].

Modeling of the didactic head shapes. The head models were further processed in SolidWorks (Dassault Systèmes, SolidWorks Corporation, Waltham, Massachusetts, United States), and were produced using an Ultimaker II Plus (Ultimaker B.V., Geldermalsen, The Netherlands) using polylactic acid material (see Fig. 1).

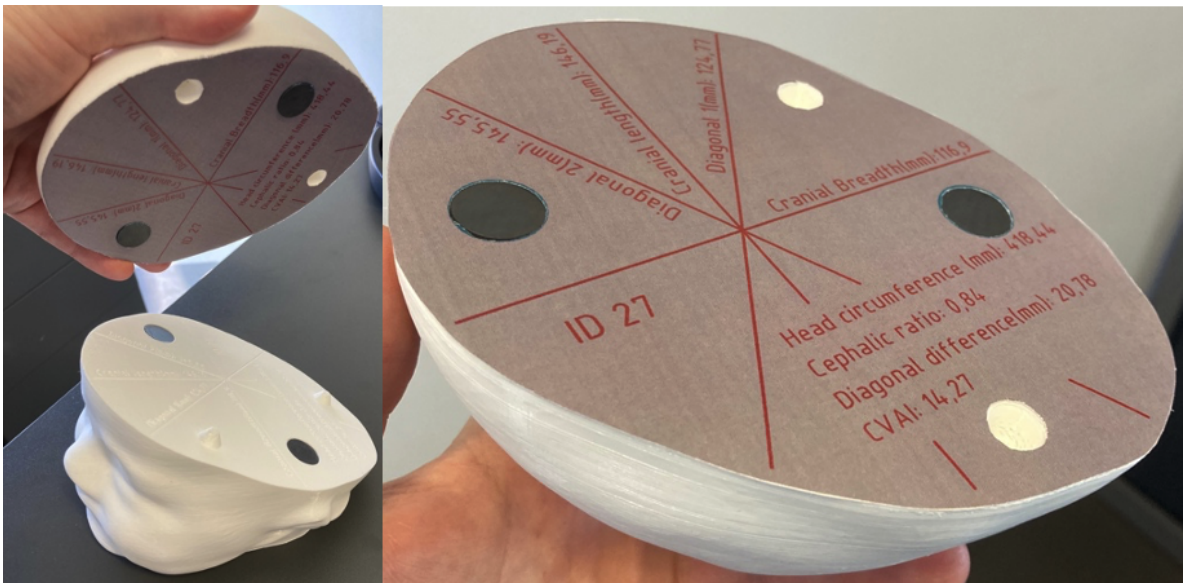

Fig. 1: Didactic head shape produced by additive manufacturing with the measurements used for the assessment of deformational plagiocephaly.

References

1. Alexandra LC Martiniuk, Cassandra Vujovich-Dunn, Miles Park, William Yu, and Barbara R Lucas. Plagiocephaly and developmental delay: a systematic review. *Journal of Developmental & Behavioral Pediatrics*, 38(1):67–78, 2017.
2. Helena R Torres, Bruno Oliveira, Pedro Morais, Anne Fritz, Fernando Veloso, Mario Rüdiqer, Jaime C Fonseca, and João L Vilaça. Developing a medical training game for visual assessment of head deformities in infants. In *2021 IEEE 9th International Conference on Serious Games and Applications for Health (SeGAH)*, pages 1–6. IEEE, 2021.
3. Patrick Fischer, Sonja Wattendorf, Seyed Amir Hossein Tabatabaei, Martina Wilbrand, Jan-Falco Wilbrand, and Keywan Sohrabi. Smartphone based monitoring of pediatric craniofacial deformities. In *Current Directions in Biomedical Engineering*, volume 8, pages 478–480. De Gruyter, 2022.
4. Helena R Torres, Pedro Morais, Anne Fritze, Wolfram Burkhardt, Maxi Kaufmann, Bruno Oliveira, Fernando Veloso, Gabriele Hahn, Mario Rüdiger, Jaime C Fonseca, et al. Anthropometric landmarking for diagnosis of cranial deformities: validation of an automatic approach and comparison with intra-and inter-observer variability. *Annals of Biomedical Engineering*, 50(9):1022–1037, 2022.